Cell Metabolism

Article

Age-related ciliopathy: Obesogenic shortening of melanocortin-4 receptor-bearing neuronal primary cilia

Graphical abstract

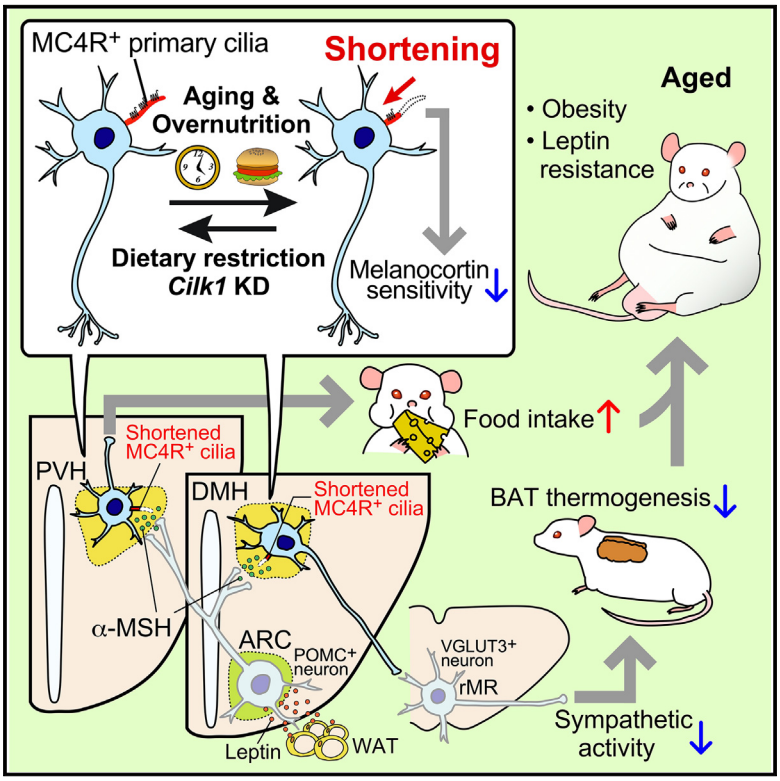

Highlights

- MC4R-bearing primary cilia (MC4R$^+$ cilia) of hypothalamic neurons shorten with age
- Shortened MC4R$^+$ cilia blunt satiety signals, leading to obesity and leptin resistance
- Chronic leptin-melanocortin signaling promotes obesogenic shortening of MC4R$^+$ cilia
- Dietary restriction or *Cilk1* knockdown reverses or inhibits MC4R$^+$ ciliary shortening

Authors

Manami Oya, Yoshiki Miyasaka, Yoshiko Nakamura, Miyako Tanaka, Takayoshi Suganami, Tomoji Mashimo, Kazuhiro Nakamura

Correspondence

kazu@med.nagoya-u.ac.jp

In brief

The melanocortin-4 receptor (MC4R) mediates leptin-melanocortin anti-obesity signaling in the hypothalamus. Oya et al. discovered that MC4R-bearing primary cilia of hypothalamic neurons progressively shorten with age to develop age-related obesity and leptin resistance. This "age-related ciliopathy" is promoted by chronic leptin-melanocortin signaling and inhibited by dietary restriction.

Oya et al., 2024, Cell Metabolism *36*, 1044–1058
May 7, 2024
https://doi.org/10.1016/j.cmet.2024.02.010

CellPress

CellPress
OPEN ACCESS

Cell Metabolism

Article

Age-related ciliopathy: Obesogenic shortening of melanocortin-4 receptor-bearing neuronal primary cilia

Manami Oya,[1] Yoshiki Miyasaka,[2] Yoshiko Nakamura,[1] Miyako Tanaka,[3,4,5] Takayoshi Suganami,[3,4,5,6] Tomoji Mashimo,[2,7,8] and Kazuhiro Nakamura[1,9,*]

[1]Department of Integrative Physiology, Nagoya University Graduate School of Medicine, Nagoya 466-8550, Japan
[2]Institute of Experimental Animal Sciences, Graduate School of Medicine, Osaka University, Osaka 565-0871, Japan
[3]Department of Molecular Medicine and Metabolism, Research Institute of Environmental Medicine, Nagoya University, Nagoya 464-8601, Japan
[4]Department of Immunometabolism, Nagoya University Graduate School of Medicine, Nagoya 466-8550, Japan
[5]Institute of Nano-Life-Systems, Institutes of Innovation for Future Society, Nagoya University, Nagoya 464-8601, Japan
[6]Center for One Medicine Innovative Translational Research (COMIT), Nagoya University, Nagoya 464-8601, Japan
[7]Division of Animal Genetics, Laboratory Animal Research Center, Institute of Medical Science, The University of Tokyo, Tokyo 108-8639, Japan
[8]Division of Genome Engineering, Center for Experimental Medicine and Systems Biology, Institute of Medical Science, The University of Tokyo, Tokyo 108-8639, Japan
[9]Lead contact
*Correspondence: kazu@med.nagoya-u.ac.jp
https://doi.org/10.1016/j.cmet.2024.02.010

SUMMARY

Obesity is often associated with aging. However, the mechanism of age-related obesity is unknown. The melanocortin-4 receptor (MC4R) mediates leptin-melanocortin anti-obesity signaling in the hypothalamus. Here, we discovered that MC4R-bearing primary cilia of hypothalamic neurons progressively shorten with age in rats, correlating with age-dependent metabolic decline and increased adiposity. This "age-related ciliopathy" is promoted by overnutrition-induced upregulation of leptin-melanocortin signaling and inhibited or reversed by dietary restriction or the knockdown of ciliogenesis-associated kinase 1 (CILK1). Forced shortening of MC4R-bearing cilia in hypothalamic neurons by genetic approaches impaired neuronal sensitivity to melanocortin and resulted in decreased brown fat thermogenesis and energy expenditure and increased appetite, finally developing obesity and leptin resistance. Therefore, despite its acute anti-obesity effect, chronic leptin-melanocortin signaling increases susceptibility to obesity by promoting the age-related shortening of MC4R-bearing cilia. This study provides a crucial mechanism for age-related obesity, which increases the risk of metabolic syndrome.

INTRODUCTION

Adult humans become increasingly susceptible to obesity through middle age. It is generally accepted that the increased susceptibility to obesity is caused by age-related alterations in energy balance, particularly a reduced resting metabolic rate in older age compared with younger age.[1] Although the age-related decline in metabolism may be partly due to reduced muscle mass,[2] age-related decline in metabolic thermogenesis in brown adipose tissue (BAT) has been strongly associated with the accumulation of body fat in middle age.[3] On the other hand, young individuals in the growth phase require more active thermogenesis to compensate for higher heat loss due to their larger body-surface-to-mass ratio. Since BAT thermogenesis is controlled by sympathetic outflow from the brain,[4] the changes in metabolic and thermogenic activities during development and aging may be ascribed to age-related alterations in the central neural circuit controlling energy homeostasis. Age-related alterations in the central circuitry may also contribute to the overeating and sedentary lifestyle that lead to adult obesity.[5] However, it is unknown how the central homeostatic circuit is altered through development and aging and whether this alteration may lead to obesity.

The melanocortin-4 receptor (MC4R) plays a pivotal role in the central neural circuit that controls the balance between energy intake and expenditure. *Mc4r* mRNA is expressed in neurons of several hypothalamic nuclei involved in the regulation of the energy balance, such as the dorsomedial hypothalamus (DMH) and the paraventricular hypothalamic (PVH) nucleus.[6] Hypothalamic MC4Rs mediate satiety signaling by the endogenous agonists, α-melanocyte-stimulating hormone (α-MSH) and β-MSH, to reduce food intake and increase energy expenditure.[7–9] This melanocortin signaling constitutes a major downstream

CellPress
OPEN ACCESS

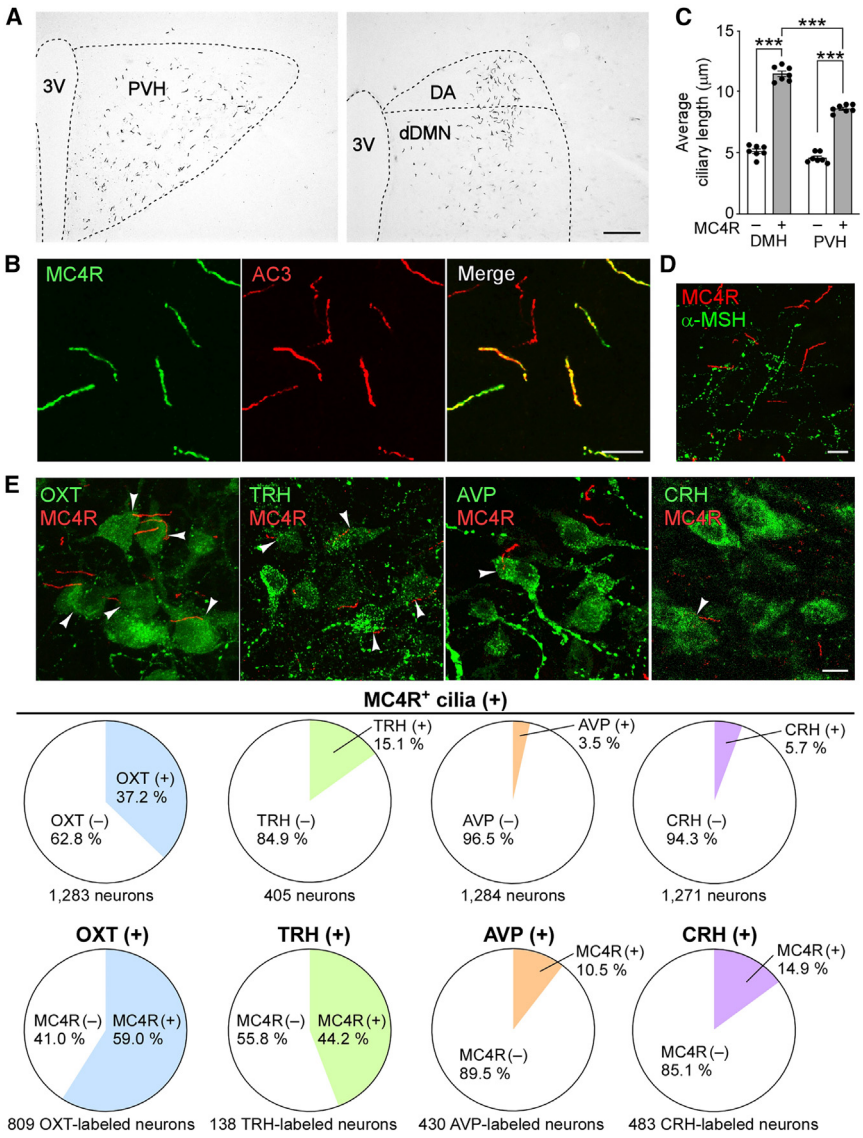

Figure 1. Endogenous MC4Rs localize to primary cilia of hypothalamic neurons

(A) MC4R immunohistochemistry in the PVH (left) and DMH (right) of 3-week-old rats using the antibody to the N terminus. 3V, third ventricle; DA, dorsal hypothalamic area; dDMN, dorsal part of the dorsomedial hypothalamic nucleus. Scale bars, 100 μm.

(B) Confocal images of MC4R-immunoreactive cilia in the DMH, which were co-labeled with AC3 immunoreactivity. Scale bars, 10 μm.

(C) Average length of MC4R-negative (AC3-positive) and MC4R-immunoreactive cilia in the DMH and PVH of 3-week-old rats (n = 7). Unpaired t test, ***$p < 0.001$. All error bars represent SEM.

(D) Close distribution of MC4R-immunoreactive cilia and α-MSH-immunoreactive axons in the PVH of 3-week-old rats. Scale bars, 10 μm. See also Video S1.

(E) Top: representative confocal images of cell bodies (arrowheads) that had MC4R-immunoreactive cilia and were immunoreactive for OXT, TRH, AVP, or CRH in the rat PVH. Scale bars, 10 μm. Bottom: populations with and without the expression of each neuropeptide in PVH neurons with MC4R-immunoreactive cilia (top) and populations with and without MC4R-immunoreactive cilia in each neuropeptidergic group of neurons (bottom). Cells were counted in 3 rats.

component of the anorexigenic leptin signaling,[10] and deficiency of the *Mc4r* gene in mice and humans results in hyperphagia and severe obesity.[11–13] However, alterations in the intracellular dynamics of MC4R proteins during development and aging have not been studied due to the unavailability of anti-MC4R antibodies applicable to the immunocytochemical detection of endogenous MC4R proteins. In a recent attempt to visualize green fluorescent protein (GFP)-tagged MC4Rs in a genetically engineered mouse model,[14] there was a concern that the exogenous addition of GFP to the intracellular C terminus of the receptor might have disrupted its physiological subcellular localization and signaling function.

Because energy intake and expenditure must be regulated commensurately with body size, it is particularly important to investigate whether the satiety signaling via hypothalamic MC4Rs is altered with development and age. If the intracellular dynamics of MC4Rs in hypothalamic neurons are altered with age, it may be relevant to the decreased thermogenic activity of BAT in middle age[3] and thereby cause age-related obesity, a risk factor for metabolic syndrome.[15,16] To investigate age-related changes in the intracellular dynamics of MC4R proteins, in this study, we developed anti-MC4R antibodies and performed immunostaining in the brains of rats of different ages under different nutritional conditions. Furthermore, using genetic approaches in rats, we investigated the extent to which age-related alterations in the intracellular dynamics of MC4R proteins affect energy homeostasis and susceptibility to obesity. Finally, to explore molecular interventions to prevent age-related obesity, we investigated the molecular signaling by which aging and nutritional conditions alter the intracellular dynamics of MC4R proteins.

RESULTS

MC4Rs localize to neuronal primary cilia

We developed two polyclonal antibodies against the N and C termini of the rat MC4R protein, which exhibited immunoreactivity to MC4R proteins expressed in cultured cells (Figure S1A). With either antibody, intense immunoreactivity was observed in fibrous structures in the DMH and PVH of rats and mice, but not in *Mc4r*-deficient mice (Figures 1A, S1B, and S1C), indicating that these antibodies specifically recognize endogenous MC4R proteins. The MC4R-immunoreactive fibrous structures were found to be neuronal primary cilia, cellular antennae,[17] as they were immunopositive for the neuronal ciliary marker, adenylate

cyclase 3 (AC3) (Figure 1B). Furthermore, these MC4R-bearing (MC4R$^+$) primary cilia were longer than MC4R-negative primary cilia in 3-week-old rats, and MC4R$^+$ cilia in the DMH were longer than those in the PVH (Figure 1C).

MC4R$^+$ primary cilia were densely distributed in the DMH and PVH (Figure 1A), but not in other brain and spinal regions in 9-week-old rats, except that some MC4R$^+$ cilia were sparsely distributed in the medial preoptic nucleus, which controls sexual behavior (Figure S1D). This observation suggests that the more broadly distributed cell populations reported to express *Mc4r* mRNA[6] or to be labeled in *Mc4r*-Cre mice[18] do not necessarily express MC4R proteins. Many axon terminals containing α-MSH were distributed in proximity to MC4R-immunoreactive primary cilia in the DMH and PVH but scarcely formed synapse-like apposition to those cilia (Figure 1D; Video S1), suggesting the role of MC4R$^+$ primary cilia as cellular antennae that receive α-MSH by volume transmission. In the following MC4R immunostaining, we used the antibody to the N terminus due to its better staining performance.

Characterization of MC4R$^+$-ciliated neurons

The PVH harbors several types of neurons that express neuropeptides, such as oxytocin (OXT), thyrotropin-releasing hormone (TRH), arginine vasopressin (AVP), and corticotropin-releasing hormone (CRH). In the PVH of 3-week-old rats, 37% of MC4R-immunoreactive primary cilia protruded from OXT neurons, and 15% were from TRH neurons, but few were from AVP and CRH neurons (Figure 1E). MC4R-immunoreactive primary cilia were observed in 59% of OXT neurons and 44% of TRH neurons but only in approximately 10% of AVP and CRH neurons (Figure 1E).

The DMH consists of the dorsomedial hypothalamic nucleus and dorsal hypothalamic area (DA)[19] (Figure 1A) and contains densely clustered neurons that send sympathoexcitatory signals to the rostral medullary raphe region (rMR).[4,20] The rMR, including the rostral raphe pallidus and raphe magnus nuclei, harbors vesicular glutamate transporter (VGLUT) 3-expressing sympathetic premotor neurons, ∼85% of which oligosynaptically innervate BAT.[4,21] To examine whether DMH→rMR projection neurons have MC4R$^+$ primary cilia, we performed retrograde neural tracing by injecting cholera toxin b-subunit (CTb), a retrograde tracer, into the rMR in 9- to 11-week-old rats (Figure 2A). MC4R-immunoreactive cilia were observed in 79% of CTb-labeled DMH neurons, and 74% of DMH neurons with MC4R-immunoreactive cilia were labeled with CTb (Figures 2A and S2A), raising the possibility that MC4R$^+$-ciliated DMH neurons innervate sympathetic premotor neurons in the rMR.

To examine this possibility by visualizing axonal projections from MC4R-expressing DMH neurons to the rMR, we developed an *Mc4r*-Cre knockin rat (Figure S2B). Injection of a Cre-reporting adeno-associated virus (AAV) (AAV-dsRed-pSico-scramble)[22] into the PVH and DMH of 3- to 4-week-old *Mc4r*-Cre rats resulted in 93% (PVH) and 87% (DMH) of Cre-expressing cells, but few Cre-negative cells, having MC4R-immunoreactive cilia (Figures S2C–S2E), indicating selective Cre recombination in MC4R-expressing cells in this rat line. AAV-mediated transduction of MC4R-expressing DMH neurons with palmitoylated GFP (palGFP), a membrane-targeted form of GFP,[23] in this rat line visualized their numerous nerve endings in the rMR, which were closely associated with VGLUT3-expressing neurons (Figures 2B and S2F). This observation suggests that MC4R$^+$-ciliated DMH neurons directly innervate sympathetic premotor neurons in the rMR to stimulate sympathetic responses, including BAT thermogenesis.

MC4Rs in DMH stimulate BAT thermogenesis via rMR

We then hypothesized that the melanocortin-sensitized DMH→rMR pathway stimulates BAT thermogenesis. However, to our knowledge, it was unknown whether melanocortin action on MC4Rs in the DMH stimulates BAT thermogenesis. Therefore, we first nanoinjected melanotan-2 (MTII), an MC4R agonist, into the DMH (Figure 2C) and examined the effects on BAT thermogenic, metabolic, and cardiac functions in anesthetized rats aged 9–11 weeks. Unilateral nanoinjection of MTII into the DMH increased BAT sympathetic nerve activity (SNA), BAT temperature (T_{BAT}), expired (Exp.) CO_2, and heart rate (HR) (Figures 2D and 2E). This result demonstrates that melanocortin signaling via MC4Rs in the DMH stimulates BAT thermogenesis and a cardiac response, thereby increasing systemic energy expenditure.

Importantly, all these thermogenic and cardiac responses to MTII were abolished by a prior nanoinjection into the rMR with muscimol, a $GABA_A$ receptor agonist widely used as a neuronal inhibitor (Figures 2C–2E). In contrast, none of the MTII-evoked responses were inhibited by suppression of neurons in both periaqueductal gray and dorsal raphe nucleus (Figures S2G–S2I), the brain sites located between the DMH and the rMR and reported to be involved in the regulation of BAT thermogenesis.[24,25] Together with our anatomical observations, these physiological results strongly support the view that melanocortin action on MC4R$^+$-ciliated DMH neurons stimulates sympathoexcitatory descending transmission via rMR premotor neurons to increase systemic energy expenditure via BAT thermogenesis and a cardiac response.

MC4R$^+$ primary cilia shorten with age

Interestingly, we noticed that MC4R$^+$ primary cilia almost disappeared in aged obese rats. Therefore, the length of MC4R-immunoreactive primary cilia of DMH and PVH neurons was examined in individually caged, wild-type male rats of various ages under different nutritional conditions. In rats fed *ad libitum* with normal chow (NC), the total length of MC4R-immunoreactive cilia in a confocal microscopic field of view (291 μm square, 25 μm thick) (Figure S3) was drastically reduced in both DMH and PVH with age after weaning at 3 weeks old until 24 weeks (Figures 3A and S4A). MC4R immunoreactivity was clearly detected along the entire length of each MC4R$^+$ primary cilium visualized by AC3 immunoreactivity, even during age-related shortening (Figures 1B and S4B), indicating that ciliary shortening reduced the number of cell-surface MC4R proteins in proportion to the length. However, *Mc4r* mRNA expression levels were comparable between 3- and 24-week-old rats in both brain regions (Figure S4C). Importantly, the total length of MC4R-negative primary cilia in the same microscopic field did not change over the time course (Figure 3A), indicating that age-related shortening occurs selectively in MC4R$^+$ primary cilia. MC4R$^+$ cilia did not exhibit circadian changes in their length (Figure S4D), unlike the suprachiasmatic nucleus.[26]

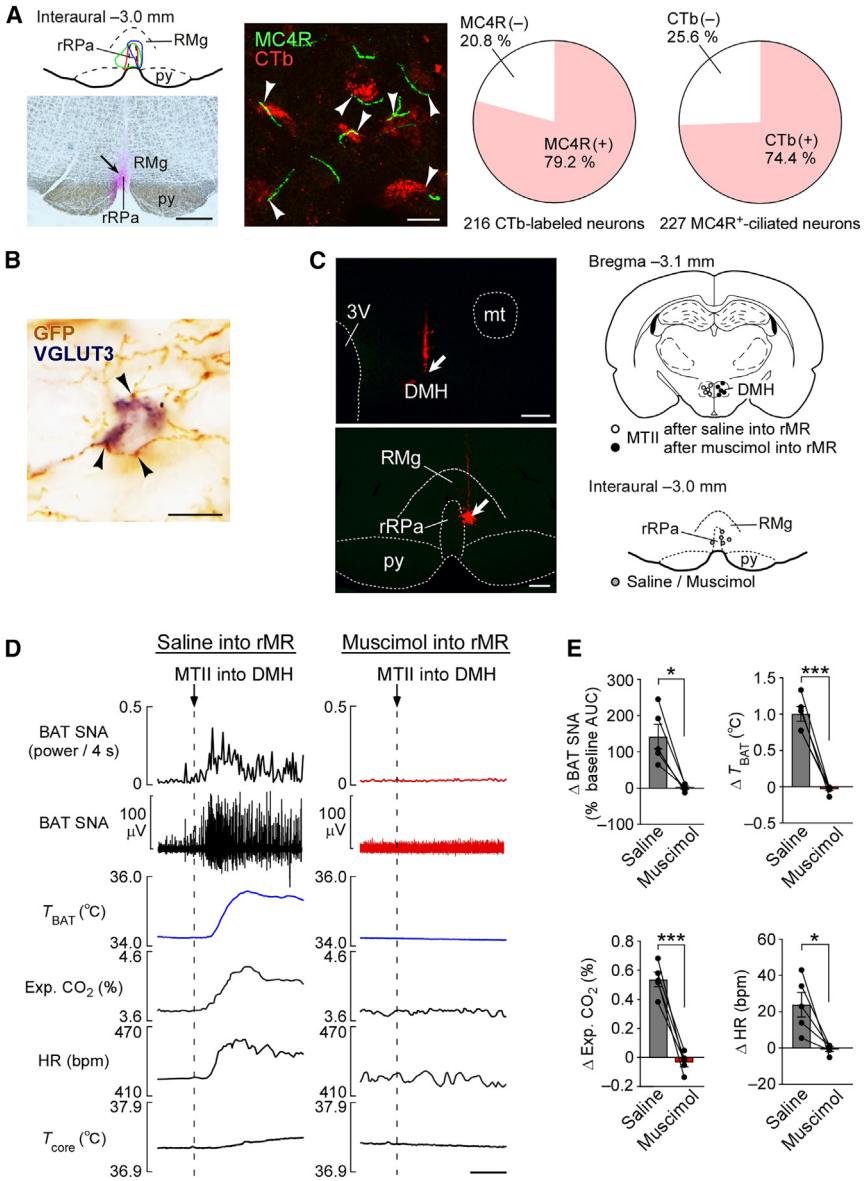

Figure 2. MC4R$^+$-ciliated DMH neurons innervate the rMR to drive BAT thermogenesis

(A) Left: CTb injection into the rMR (top, delineated by red, blue, and green lines for 3 rats). The bottom image shows a representative injection (arrow). Scale bars, 500 μm. py, pyramidal tract; RMg, raphe magnus nucleus; rRPa, rostral raphe pallidus nucleus. Middle: CTb-labeled (rMR-projecting) DMH neurons with MC4R-immunoreactive primary cilia (arrowheads). Scale bars, 10 μm. See also Figure S2A. Right: MC4R$^+$-ciliated population in CTb-labeled DMH neurons (left) and CTb-labeled population in MC4R$^+$-ciliated DMH neurons (right). Counted in 3 rats.

(B) Apposition (arrowheads) of palGFP-labeled axon swellings of MC4R-expressing DMH neurons to a VGLUT3-immunoreactive cell body in the rMR. Scale bars, 10 μm. See also Figure S2F.

(C–E) *In vivo* physiological experiments. The effect of MTII nanoinjection into the DMH (unilateral) was tested after saline and muscimol nanoinjection into the rMR in the same anesthetized rats (injection sites mapped in C). Arrows (C) show representative injections identified with fluorescent microbeads. Scale bars, 200 μm. mt, mammillothalamic tract. MTII injection (arrow, D) into the DMH increased BAT SNA, T_{BAT}, Exp. CO_2, and HR after saline injection, but not after muscimol injection into the rMR in the same rat. Timescale, 100 s. Group data (E) compare MTII-evoked changes (means ± SEM of 5 rats) by paired t tests. *$p < 0.05$ and ***$p < 0.001$.

In rats fed *ad libitum* with high-fat diet (HFD) from 3 weeks old, MC4R-immunoreactive cilia shortened similarly in the DMH and a little faster in the PVH compared with the NC-fed group (Figure 3A). In contrast, NC feeding with dietary restriction (DR: fed 60% of consumption by *ad libitum* NC-fed rats of the same age) from 3 weeks old strongly inhibited the shortening of MC4R-immunoreactive cilia in both brain regions (Figure 3A). Therefore, MC4R$^+$ primary cilia in hypothalamic neurons shorten with age, and this is promoted by overnutrition and inhibited by undernutrition.

In even older male rats (6–20 months old), which were group reared with *ad libitum* NC feeding, the length of MC4R-immunoreactive cilia of DMH and PVH neurons was kept short, whereas that of MC4R-negative cilia remained unchanged (Figure 3B). Interestingly, postnatal histochemical analyses revealed that MC4R-immunoreactive cilia of DMH and PVH neurons were longest at 3 weeks old (Figure S4E), the average weaning time for rats. Soon after weaning, infants are at risk of hypothermia because they no longer acquire heat from the dam and easily lose body heat due to the high surface-area-to-mass ratio of their small body. Therefore, they particularly need a high ability to actively produce heat. Consistently, oxygen consumption per body weight, indicative of energy expenditure, was 2.5–3.5 times higher in 3-week-old rats than in adults (Figure 3C). Since MC4R$^+$-ciliated DMH neurons directly innervate BAT sympathetic premotor neurons (Figure 2B), we examined whether the length of MC4R$^+$ cilia in DMH neurons is correlated with metabolic parameters. The shortening of MC4R-immunoreactive cilia of DMH neurons after weaning was correlated with age-related decreases in body-surface-area-to-mass (weight) ratio and oxygen consumption (Figures 3D, 3E, and S4F). In the whole cohort, including the NC, HFD, and DR groups, the length of MC4R-immunoreactive cilia in the DMH was negatively correlated with body fat percentage (Figure 3F). These results raise the possibility that MC4R$^+$ primary cilia of DMH neurons are shortened to regulate the amount of thermogenesis commensurate with body size during the developmental phase, whereas the resultant reduction in the sensitivity of DMH neurons to melanocortins results in the accumulation of body fat in adults.

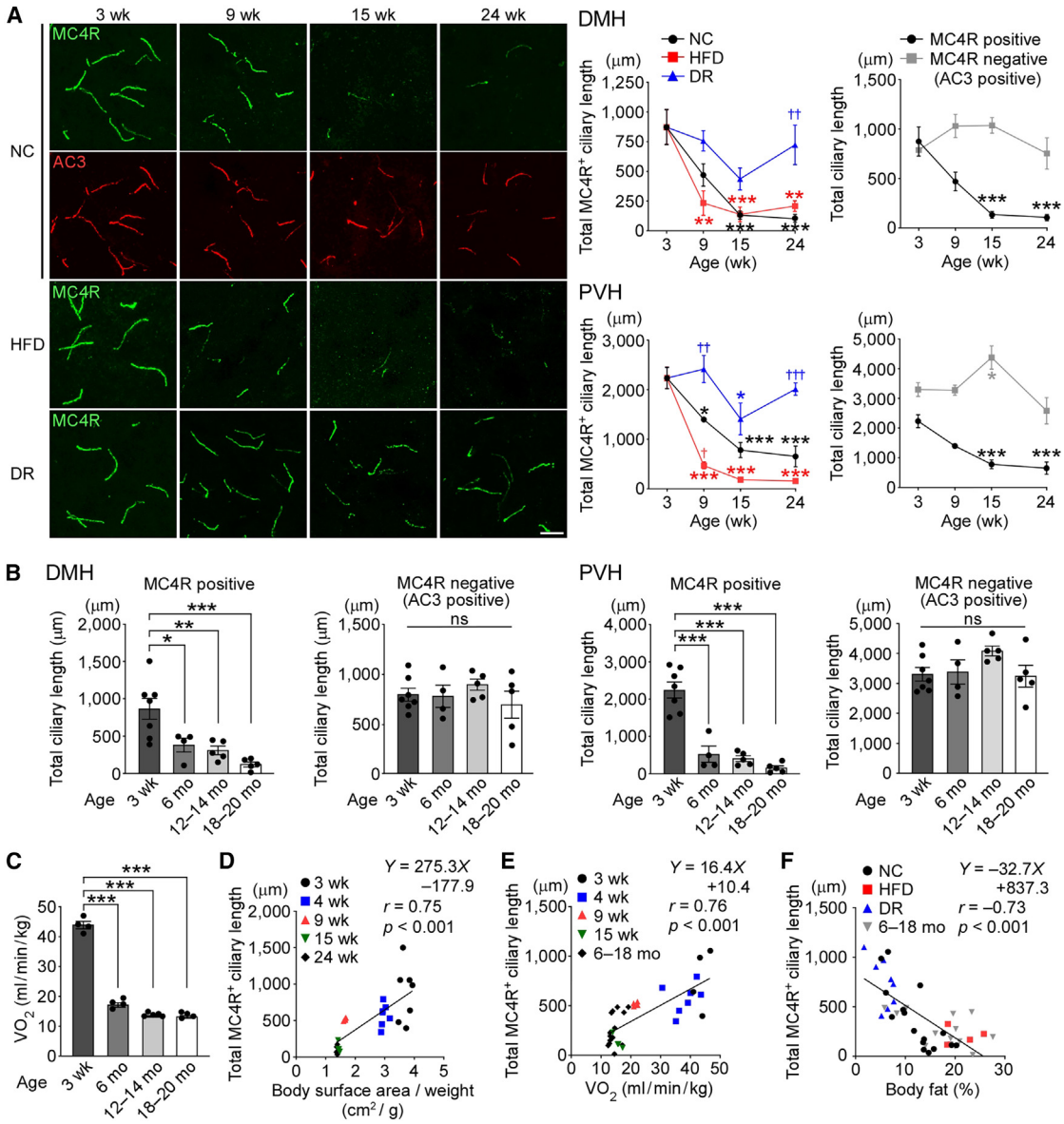

Figure 3. MC4R+ primary cilia shorten with age in correlation with metabolic decline and increased adiposity

(A) Left: MC4R-immunoreactive cilia in the DMH of 3- to 24-week-old, individually caged rats fed with *ad libitum* normal chow (NC), *ad libitum* high-fat diet (HFD), or normal chow with dietary restriction (DR). Scale bars, 10 μm. Right: age-related changes in the length of MC4R-immunoreactive cilia in the DMH and PVH (left graphs, n = 4 rats except 3-week-old rats, n = 7). Right graphs compare MC4R-immunoreactive and MC4R-negative (AC3-immunopositive) cilia in the NC group. Two-way ANOVA followed by Bonferroni's post hoc test, *p < 0.05, **p < 0.01, and ***p < 0.001 (vs. 3 weeks old); †p < 0.05, ††p < 0.01, and †††p < 0.001 (vs. NC).

(B) Length of MC4R-immunoreactive and MC4R-negative (AC3-positive) cilia of group-caged, NC-fed rats over 6 months old (n = 4–5), compared with 3-week-old rats from (A) (n = 7). One-way ANOVA followed by Bonferroni's post hoc test, *p < 0.05; **p < 0.01; and ***p < 0.001; ns, not significant.

(C) Metabolic rate (VO_2, oxygen consumption rate per body weight) in rats over 6 months old, compared with 3-week-old rats (n = 4–5). One-way ANOVA followed by Bonferroni's post hoc test, ***p < 0.001.

(D–F) Linear regression analyses (Pearson's correlation tests) between MC4R+ ciliary length in the DMH and the ratio of body surface area to body weight of NC rats (D); VO_2 of NC rats (E); or body fat percentage of NC, HFD, and DR rats (F). The rats aged 6–18 months in (B) and (C) were also included (6–18 months). All error bars represent SEM.

We also confirmed that MC4R+ primary cilia of both DMH and PVH neurons in female rats (group reared with *ad libitum* NC feeding) were shortened from 3 to 24 weeks of age to a similar extent as in males (Figure S4G). These data indicate that the age-related reduction in melanocortin sensitivity dependent on MC4R+ ciliary shortening occurs similarly in both sexes. Therefore, the following experiments were performed in male rats to minimize the number of animals sacrificed.

Shortening of MC4R+ cilia is obesogenic

To determine the contribution of hypothalamic MC4R+ cilia to energy balance regulation, we selectively shortened MC4R+ primary

cilia in specific brain regions by knocking down the expression of intraflagellar transport protein 88 (*Ift88*) mRNA. IFT88 is a subunit of the IFT-B complex, which plays an important role in the anterograde transport of ciliary proteins.[27,28] In preliminary experiments, two short hairpin RNAs (*Ift88* shRNA #1 and #2) or a scramble sequence was expressed in nonspecific DMH and PVH neurons with AAVs at 3 weeks of age, and 2 weeks later, the expression of either shRNA, but not the scramble, efficiently shortened primary cilia and eliminated IFT88 protein in infected neurons (Figures S5A and S5B). Following this validation, we selected *Ift88* shRNA #1 and generated an AAV for Cre-dependent expression of the shRNA (AAV-dsRed-pSico-*Ift88* shRNA). The AAV was injected bilaterally into both DMH and PVH of 9-week-old *Mc4r*-Cre rats, which were then fed NC *ad libitum* for 7 weeks. The expression of *Ift88* shRNA markedly shortened MC4R$^+$ cilia in 2–4 weeks after AAV injection and almost eliminated them at 7 weeks in both hypothalamic nuclei but did not affect MC4R-negative primary cilia (Figures 4A and S5C). The expression of *Ift88* shRNA also did not cause appreciable cytotoxicity or cell death, as it did not affect the number of *Mc4r*-Cre-positive cells (Figure S5D). The *Ift88*-knockdown (KD) rats exhibited significantly lower oxygen consumption and higher food intake than control rats in which an AAV with a scramble sequence instead of shRNA (AAV-dsRed-pSico-scramble) was injected into the DMH and PVH (Figures 4B and 4C). Consequently, the *Ift88*-KD rats exhibited remarkably greater increases in body weight and adiposity than the scramble rats (Figure 4D). Therefore, the shortening of MC4R$^+$ primary cilia in DMH and PVH neurons exerts strong obesogenic effects by reducing systemic metabolism and increasing food intake.

To more specifically determine the role of MC4R$^+$ primary cilia of DMH neurons in energy homeostasis, AAV-dsRed-pSico-*Ift88* shRNA was bilaterally injected only into the DMH of 9-week-old *Mc4r*-Cre rats, resulting in extremely shortened MC4R-immunoreactive cilia in the DMH (Figure 4E). These rats exhibited lower oxygen consumption but consumed comparable amounts of food compared with scramble rats (Figures 4F and 4G). Nonetheless, these *Ift88*-KD rats exhibited greater increases in body weight and adiposity than scramble rats (Figure 4H). These results indicate that ciliary MC4Rs in DMH neurons mediate melanocortin signaling to increase energy expenditure, but not to decrease food intake, and that the shortening of MC4R$^+$ cilia in DMH neurons has a sufficient obesogenic impact.

Shortening of MC4R$^+$ cilia blunts BAT thermogenesis and cold defense

To examine the behavioral effects of shortening MC4R$^+$ cilia, *Mc4r*-Cre rats with *Ift88* KD in MC4R$^+$-ciliated DMH and PVH neurons were implanted with a telemetric transmitter for daily monitoring of activity, body core temperature (T_{core}), and T_{BAT}. They exhibited daily changes in activity and T_{core} comparable to scramble rats but had slightly lower T_{BAT} (Figures S5E–S5G). Interestingly, the elevation of T_{BAT} observed in scramble rats during cold exposure was not evident in *Ift88*-KD rats (Figure S5G), indicating that the shortening of MC4R$^+$ primary cilia blunts adaptive BAT thermogenesis for cold defense.

We further determined the impact of shortening MC4R$^+$ cilia in DMH neurons on BAT thermogenic and cardiac functions in anesthetized rats. Similar to wild-type rats (Figures 2C–2E), the unilateral nanoinjection of MTII into the DMH of control (scramble AAV-injected) *Mc4r*-Cre rats aged 11–13 weeks increased BAT SNA, T_{BAT}, Exp. CO_2, and HR (Figures 5A and 5B). However, all these thermogenic, metabolic, and cardiac responses to MTII were abolished by shortening MC4R$^+$ cilia of DMH neurons with *Ift88* KD in *Mc4r*-Cre rats of the same age (2–4 weeks after AAV injection; Figures 5A, 5B, S6A, and S6B). These results demonstrate that ciliary MC4R proteins in DMH neurons are essential for the action of melanocortins to elicit BAT thermogenic and cardiac responses and, importantly, that neurons with shortened MC4R$^+$ primary cilia lose the responsiveness to melanocortin inputs.

Notably, aged animals similarly exhibited a reduced responsiveness of DMH neurons to melanocortins. Although the unilateral nanoinjection of MTII into the DMH of 9-week-old wild-type rats (Figure S6C) elicited marked increases in BAT SNA, T_{BAT}, Exp. CO_2, and HR, these responses were blunted in 6-month-old (~24 weeks) rats (Figures 5C and 5D), which had shorter MC4R$^+$ cilia in the DMH than 9-week-old rats (Figure 3A). Furthermore, BAT thermogenic and tachycardic responses evoked by trunk skin cooling were significantly smaller in rats with artificially (*Ift88*-KD rats) or age-dependently (6-month-old rats) shortened MC4R$^+$ primary cilia in the DMH than in the respective control rats (Figures 5E and 5F). Therefore, melanocortin signaling via ciliary MC4Rs in DMH neurons strongly supports central sympathetic outflow to drive cold-defensive responses. The age-related shortening of MC4R$^+$ primary cilia of DMH neurons reduces the capability for BAT thermogenesis, thereby contributing to the reduced whole-body metabolic rate and blunted cold defense in aged animals.

Shortening of MC4R$^+$ cilia causes leptin resistance

Leptin is an adipokine that suppresses appetite by activating proopiomelanocortin (POMC) neurons in the arcuate nucleus of the hypothalamus, and MC4Rs mediate the leptin-elicited melanocortin signaling from POMC neurons to reduce food intake.[7–9,29] Leptin resistance is a hallmark of obesity and metabolic syndrome, but its etiology remains unclear.[29,30] To test the hypothesis that the age-related shortening of MC4R$^+$ primary cilia in hypothalamic neurons contributes to the development of leptin resistance, we examined leptin sensitivity in rats with shortened MC4R$^+$ cilia. Leptin injection into the lateral ventricle reduced food intake in control (scramble AAV-injected) *Mc4r*-Cre rats at 10 weeks of age, whereas this leptin effect was abolished in *Ift88*-KD rats with shortened MC4R$^+$ cilia in both PVH and DMH or even only in the PVH (Figures 6A, S7A, and S7B). Therefore, the shortening of MC4R$^+$ cilia in hypothalamic neurons, particularly PVH neurons, causes leptin resistance in feeding regulation by disrupting the leptin-melanocortin signaling pathway.

Leptin signaling shortens MC4R$^+$ cilia

To further investigate the mechanistic relationship between the age-related shortening of MC4R$^+$ primary cilia and obesity, we examined the length of MC4R$^+$ cilia in obese Zucker *fa*/*fa* rats, an outbred strain that harbors a missense mutation (*fa*) in the leptin receptor (LepR) gene and exhibits blunted leptin signaling.[31] Given their severe obesity, we initially expected this strain to

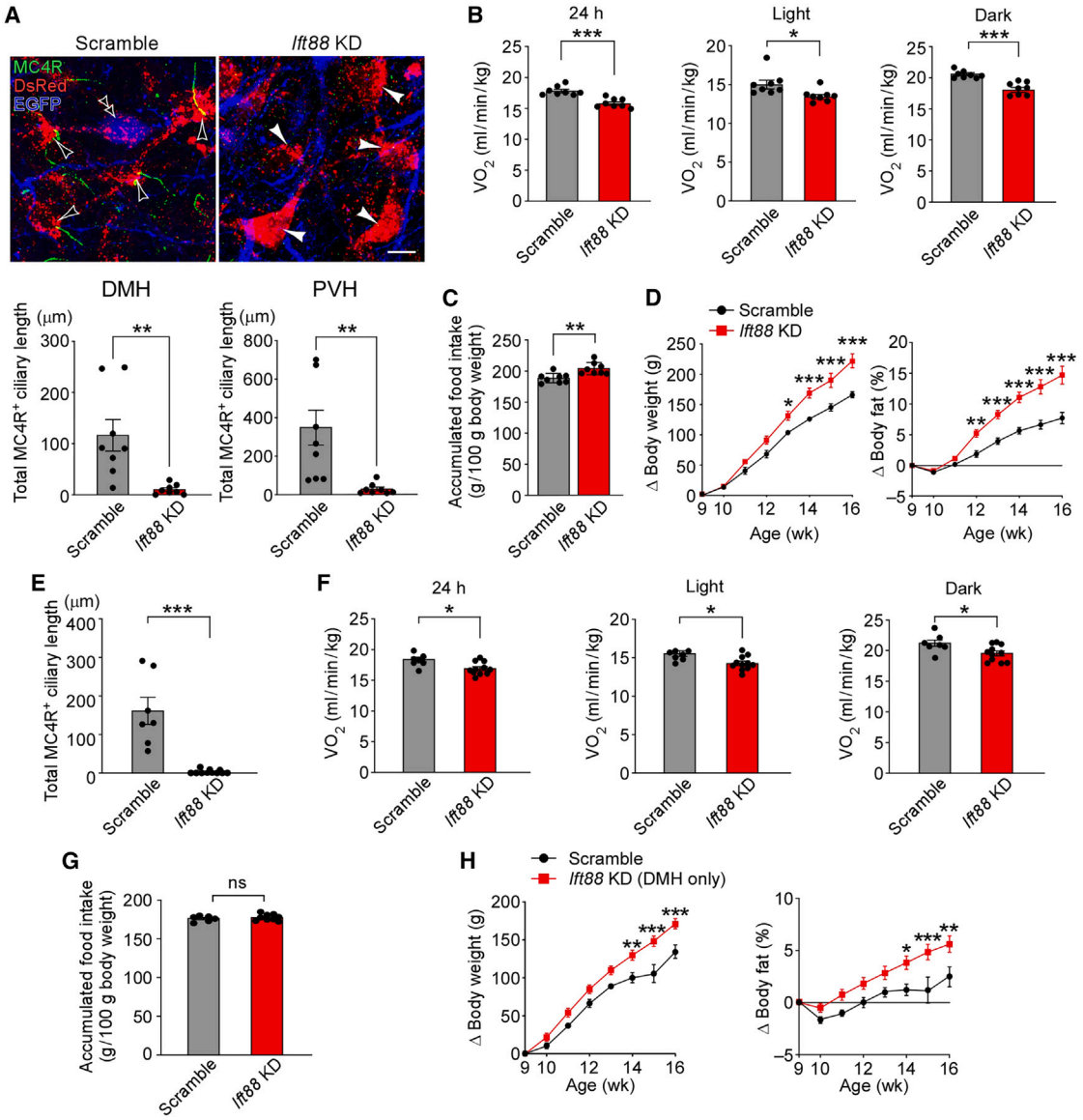

Figure 4. Shortening of MC4R$^+$ cilia is obesogenic

(A) *Ift88* KD shortens MC4R$^+$ cilia. AAV-dsRed-pSico-scramble (scramble) or AAV-dsRed-pSico-*Ift88* shRNA (*Ift88* KD) was bilaterally injected into the DMH and PVH of 9-week-old *Mc4r*-Cre rats. Pseudocolored images of infected DMH neurons 7 weeks after AAV injection (top) show that *Mc4r*-Cre-expressing neurons, labeled with dsRed only (single arrowheads), had MC4R-immunoreactive cilia in scramble rats, whereas those cilia were extremely shortened or eliminated in *Ift88*-KD rats. *Mc4r*-Cre-negative neurons, labeled with both dsRed and EGFP (double arrowheads), did not have MC4R-immunoreactive cilia (see also Figure S5C). Scale bars, 10 μm. Graphs (bottom) show the total length of MC4R-immunoreactive cilia 7 weeks after AAV injection (n = 8 rats). Unpaired t test, $^{**}p < 0.01$.

(B) *Ift88* KD reduces metabolic rate. Average readings of VO_2 for a 24-h period, light phase or dark phase 7 weeks after AAV injection (n = 8). Unpaired t test, $^{*}p < 0.05$ and $^{***}p < 0.001$.

(C) *Ift88* KD increases food intake. Weekly food intake (total of 7 days) was calculated per 100 g unit of weekly body weight and summed for 7 weeks after AAV injection (n = 8). Unpaired t test, $^{**}p < 0.01$.

(D) *Ift88*-KD rats exhibit greater increases in body weight and adiposity. Body weight and body fat percentage were measured weekly for 7 weeks after AAV injection (n = 8). Two-way ANOVA followed by Bonferroni's post hoc test, $^{*}p < 0.05$, $^{**}p < 0.01$, and $^{***}p < 0.001$.

(E–H) AAV-dsRed-pSico-scramble (scramble) or AAV-dsRed-pSico-*Ift88* shRNA (*Ift88* KD) was bilaterally injected into the DMH, but not into the PVH, of 9-week-old *Mc4r*-Cre rats (scramble, n = 7; *Ift88* KD, n = 11; except G, scramble, n = 6; *Ift88* KD, n = 9). 7 weeks after AAV injection, MC4R-immunoreactive cilia in the DMH were shortened by *Ift88* KD (E). *Ift88*-KD rats exhibited reduced metabolic rate (F), but intact food intake (G), contrasting to the increased food intake by *Ift88* KD in both PVH and DMH (C). Unpaired t test (E–G), $^{*}p < 0.05$; $^{***}p < 0.001$; ns, not significant. *Ift88*-KD rats exhibited greater increases in body weight and adiposity (H, two-way ANOVA followed by Bonferroni's post hoc test, $^{*}p < 0.05$, $^{**}p < 0.01$, and $^{***}p < 0.001$).

All error bars represent SEM.

CellPress
OPEN ACCESS

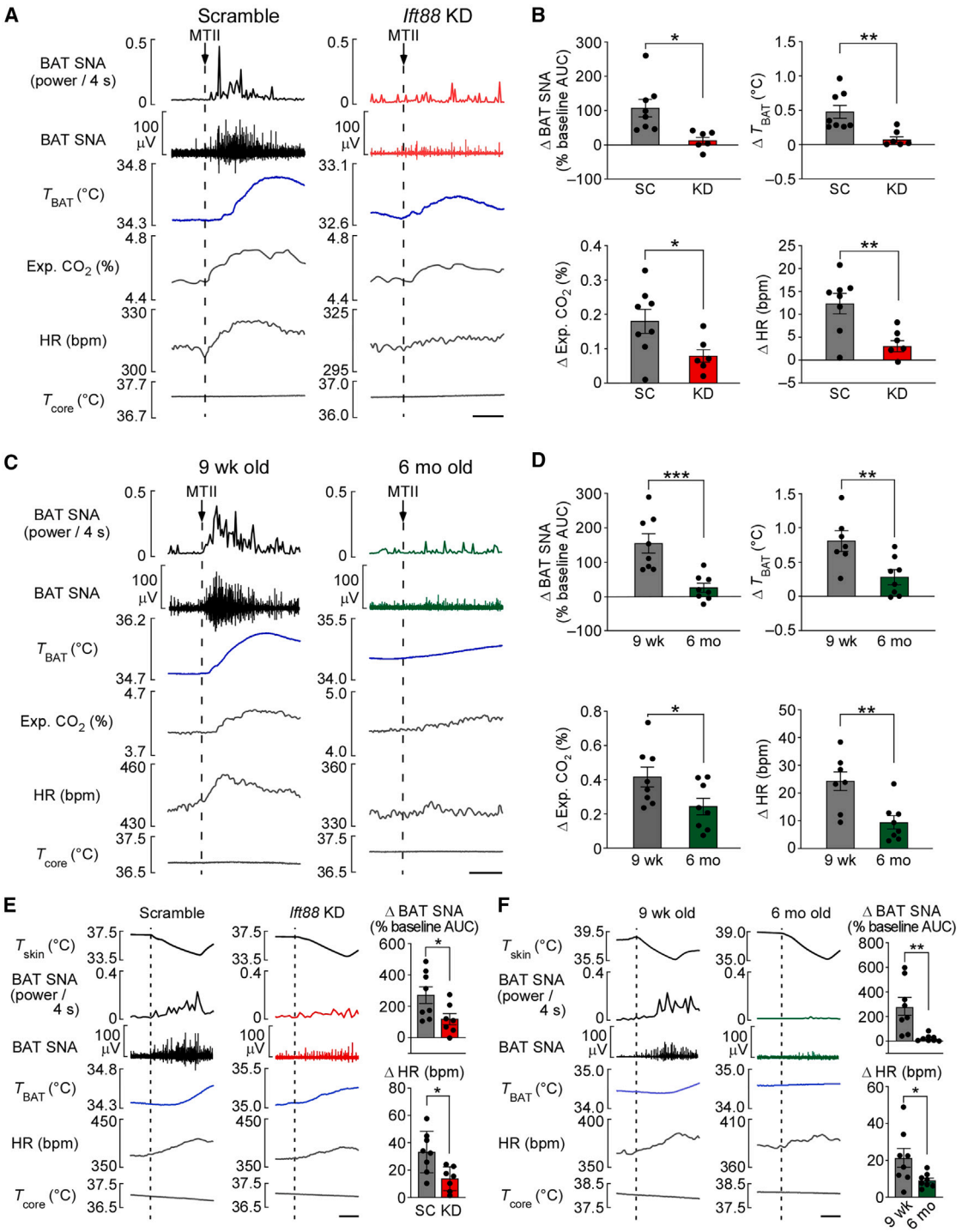

Figure 5. Shortening of MC4R$^+$ cilia in DMH neurons blunts BAT thermogenesis and cold defense

(A–D) Shortening of MC4R$^+$ cilia blunts the sensitivity of thermogenic DMH neurons to melanocortin signals. In (A) and (B), scramble or *Ift88*-KD AAV was injected into the DMH of 9-week-old *Mc4r*-Cre rats, and *in vivo* physiological recordings were performed at 11–13 weeks old. Unilateral MTII nanoinjection into the DMH (arrows) increased BAT SNA, T_{BAT}, Exp. CO_2, and HR in scramble rats (SC, A and B) and 9-week-old wild-type rats (C and D), but the responses were diminished in *Ift88*-KD rats (KD, A and B) and 6-month-old wild-type rats (C and D). Timescales, 100 s. MTII-evoked changes are compared by unpaired t tests (B and D, n = 6–8). *p < 0.05, **p < 0.01, and ***p < 0.001. See also Figure S6.

(E and F) Shortening of MC4R$^+$ cilia blunts cooling-evoked BAT thermogenic and cardiac responses. Skin cooling (T_{skin}) was given to scramble and *Ift88*-KD rats (E) and 9-week-old and 6-month-old wild-type rats (F) (n = 7–8). Timescale, 30 s. Unpaired t test, *p < 0.05 and **p < 0.01.

All error bars represent SEM.

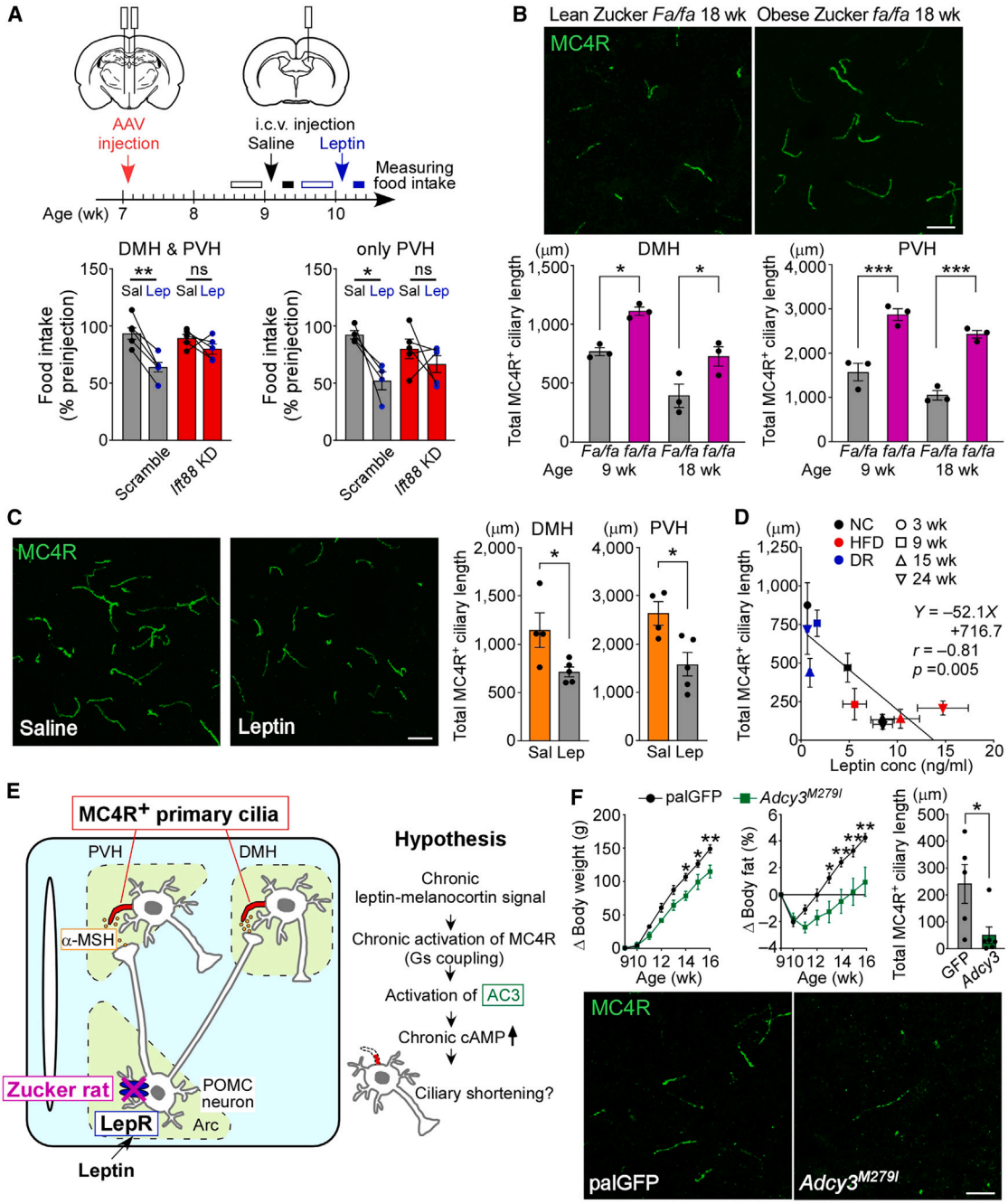

Figure 6. Chronic leptin-melanocortin signaling shortens MC4R$^+$ cilia, and shortening MC4R$^+$ cilia causes leptin resistance

(A) *Ift88* KD induces leptin resistance. Top: scramble or *Ift88*-KD AAV was injected into both DMH and PVH or only the PVH of *Mc4r*-Cre rats (n = 4–5) at 7 weeks old. Saline and leptin were injected into the lateral ventricle (i.c.v.) 2 and 3 weeks later, respectively. Bottom: food intake after i.c.v. injection is expressed as a percentage of preinjection food intake. Paired t test; *p < 0.05; **p < 0.01; ns, not significant. See also Figures S7A and S7B.

(B) Ablation of leptin signaling inhibits the age-related shortening of MC4R$^+$ cilia. Top: MC4R-immunoreactive cilia in the DMH of lean and obese Zucker rats. Scale bars, 10 μm. Bottom: MC4R-immunoreactive cilia were longer in obese Zucker rats (n = 3). One-way ANOVA followed by Bonferroni's post hoc test, *p < 0.05 and ***p < 0.001.

(C) Chronic leptin signaling shortens MC4R$^+$ cilia. Wild-type rats (12 weeks old) were injected with saline (n = 4) or leptin (5 μg, n = 5) into the lateral ventricle every other day for 5 weeks under DR (fed 60% of NC consumed by *ad-libitum*-fed, age-matched rats). Leptin injection shortened MC4R-immunoreactive cilia in both DMH (left images) and PVH. Scale bars, 10 μm. Unpaired t test; *p < 0.05.

(D) Serum leptin concentration negatively correlates with MC4R$^+$ ciliary length. Linear regression analysis (Pearson's correlation test) between MC4R$^+$ ciliary length in the DMH (data from Figure 3A) and serum leptin concentrations measured in wild-type rats of the same diet and age (n = 4 rats except 3-week-old NC-fed rats: ciliary length, n = 7; and leptin n = 12).

(E) Hypothetical mechanism by which chronic leptin-melanocortin signaling shortens MC4R$^+$ primary cilia. LepR, leptin receptor.

(legend continued on next page)

have short MC4R$^+$ cilia. However, obese Zucker *fa/fa* rats at 9 and 18 weeks of age had longer MC4R-immunoreactive cilia in both DMH and PVH than age-matched lean *Fa/fa* rats (Figure 6B). Therefore, the ablation of leptin-melanocortin signaling inhibits the age-related shortening of MC4R$^+$ cilia. Consistently, chronic (5 weeks) leptin injections into the lateral ventricle of wild-type rats shortened MC4R$^+$ cilia even under the DR condition (Figure 6C), despite significantly reduced body weight (saline: 298 ± 3 g, mean ± SEM of 4 rats; leptin: 242 ± 4 g, 5 rats; t_7 = 9.62, $p < 0.001$, unpaired t test). Furthermore, serum leptin levels negatively correlated with MC4R$^+$ ciliary length (Figure 6D). These results indicate that the chronic upregulation of leptin-melanocortin signaling promotes the age-related shortening of MC4R$^+$ primary cilia in hypothalamic neurons.

Because the MC4R is coupled to the stimulatory G protein G_s,[32,33] the binding of α-MSH to MC4Rs, as an outcome of leptin-melanocortin signaling, activates AC, leading to increased intracellular cyclic AMP (cAMP) levels (Figure 6E). To chronically stimulate this signaling pathway, we bilaterally injected the DMH with an AAV for Cre-dependent expression of a constitutively active mutant of AC3 (*Adcy3*^{M279I})[34] in 9-week-old *Mc4r*-Cre rats and assessed body weight and body fat percentage for 7 weeks. Because this mutant simulates chronic MC4R-mediated melanocortin satiety signaling, rats expressing *Adcy3*^{M279I} in MC4R-expressing DMH neurons were leaner than control rats expressing palGFP instead (Figure 6F). Notably, however, postmortem examination revealed that MC4R$^+$ cilia were almost lost in the DMH with *Adcy3*^{M279I} expression compared with the control group (Figure 6F). These results indicate that the chronic upregulation of leptin-melanocortin-MC4R signaling, as in obese animals, blunts the signaling itself by diminishing MC4R$^+$ cilia.

DR regenerates MC4R$^+$ cilia in aged rats

If leptin signaling shortens MC4R$^+$ cilia in hypothalamic neurons, a hunger state might regenerate eliminated MC4R$^+$ cilia in aged rats. To test this possibility, we examined the length of MC4R$^+$ cilia in the hypothalamus of 20-month-old wild-type rats after 2 months of DR (fed 60% of NC consumed by *ad-libitum*-fed control rats). Body weight and body fat percentage decreased by 13% ± 0.1% and 29% ± 2%, respectively, during DR (means ± SEM, n = 3). Control rats (18–20 months old) fed *ad libitum* with NC exhibited trace levels of MC4R-immunoreactive ciliary length in the DMH and PVH (Figure 3B). However, DR rats had significantly longer MC4R-immunoreactive cilia in both regions (Figure 7A), indicating that even once shortened, MC4R$^+$ primary cilia can regrow in old animals with DR, perhaps due to reduced leptin-melanocortin signaling.

Molecular intervention to prevent MC4R$^+$ ciliary shortening

To explore interventions to prevent age-related obesity, we attempted a molecular strategy to counteract the HFD-induced shortening of MC4R$^+$ primary cilia. The length of primary cilia is regulated by the opposing actions of anterograde and retrograde transporters, which transport membrane proteins and tubulin that constitute primary cilia.[35] Ciliogenesis-associated kinase 1 (CILK1 or intestinal cell kinase), a serine/threonine protein kinase of ciliary transporters, localizes to primary cilia to negatively regulate ciliary length,[36] and the knockdown of *Cilk1* expression accelerates anterograde intraflagellar transport in primary cilia for elongation.[37] To knock down *Cilk1* mRNA expression in MC4R-expressing hypothalamic neurons, we selected a rat *Cilk1* shRNA sequence corresponding to that used in mice[37] and injected an AAV for Cre-dependent expression of the shRNA (AAV-dsRed-pSico-*Cilk1* shRNA) bilaterally into both DMH and PVH of 9-week-old *Mc4r*-Cre rats, which were then fed HFD *ad libitum* for 7 weeks. The expression of the shRNA reduced *Cilk1* mRNA in MC4R-expressing hypothalamic neurons (Figure S7C).

MC4R$^+$ cilia were successfully maintained longer in the DMH of *Cilk1*-KD rats at 16 weeks old, in contrast to shortened MC4R$^+$ cilia in scramble rats, whereas *Cilk1* KD did not affect MC4R$^+$ cilia in the PVH for unknown reasons (Figure 7B). Nonetheless, the prevention of the age-related shortening of MC4R$^+$ primary cilia in the DMH significantly reduced body weight gain on HFD (Figure 7C). This finding indicates that the molecular machinery regulating intraflagellar transport in MC4R$^+$ primary cilia of hypothalamic neurons can be a potential target for the prevention of age-related obesity.

DISCUSSION

Obesity is a major health problem in many developed countries; therefore, combating obesity has been a major focus of health science. In this study, we discovered "age-related ciliopathy" as a key cellular mechanism in the brain that makes individuals more susceptible to obesity as they age. Our discovery that MC4R$^+$ primary cilia shorten with age to reduce the hypothalamic sensitivity to satiety signals significantly adds to the current concept of the etiology of obesity and leptin resistance. Furthermore, this study is the first to show that primary cilia of a specific group of central neurons are selectively shortened with age, providing important implications for central systems controlling other homeostatic functions that are altered with age, such as sleep, cardiovascular, and endocrine regulations. Alterations in cilia-mediated signaling pathways, such as Sonic Hedgehog and Wnt pathways, in the brain have been linked to brain diseases that progress with age, including Alzheimer's and Parkinson's diseases.[38] It would be interesting to investigate whether the age-related ciliopathy we found also occurs in other neurons and, if so, whether it is involved in age-related diseases and conditions besides obesity and leptin resistance.

Our MC4R immunohistochemistry revealed the native localization of endogenous MC4R proteins to primary cilia of DMH and PVH neurons in wild-type animals, extending the

(F) Constitutive activation of AC3 eliminates MC4R$^+$ cilia. Top left: AAV-EF1α-DIO-palGFP (palGFP) or AAV-CMV-Flex-FLAG-*Adcy3*^{M279I} (*Adcy3*^{M279I}) was bilaterally injected into the DMH of 9-week-old *Mc4r*-Cre rats (n = 5 and 6, respectively), and weekly changes in body weight and body fat percentage were analyzed by two-way ANOVA followed by Bonferroni's post hoc test (*$p < 0.05$ and **$p < 0.01$). Bottom: MC4R-immunoreactive cilia in the DMH 7 weeks after AAV injection. Scale bars, 10 μm. Top right: length of MC4R-immunoreactive cilia in the DMH. Unpaired t test, *$p < 0.05$.
All error bars represent SEM.

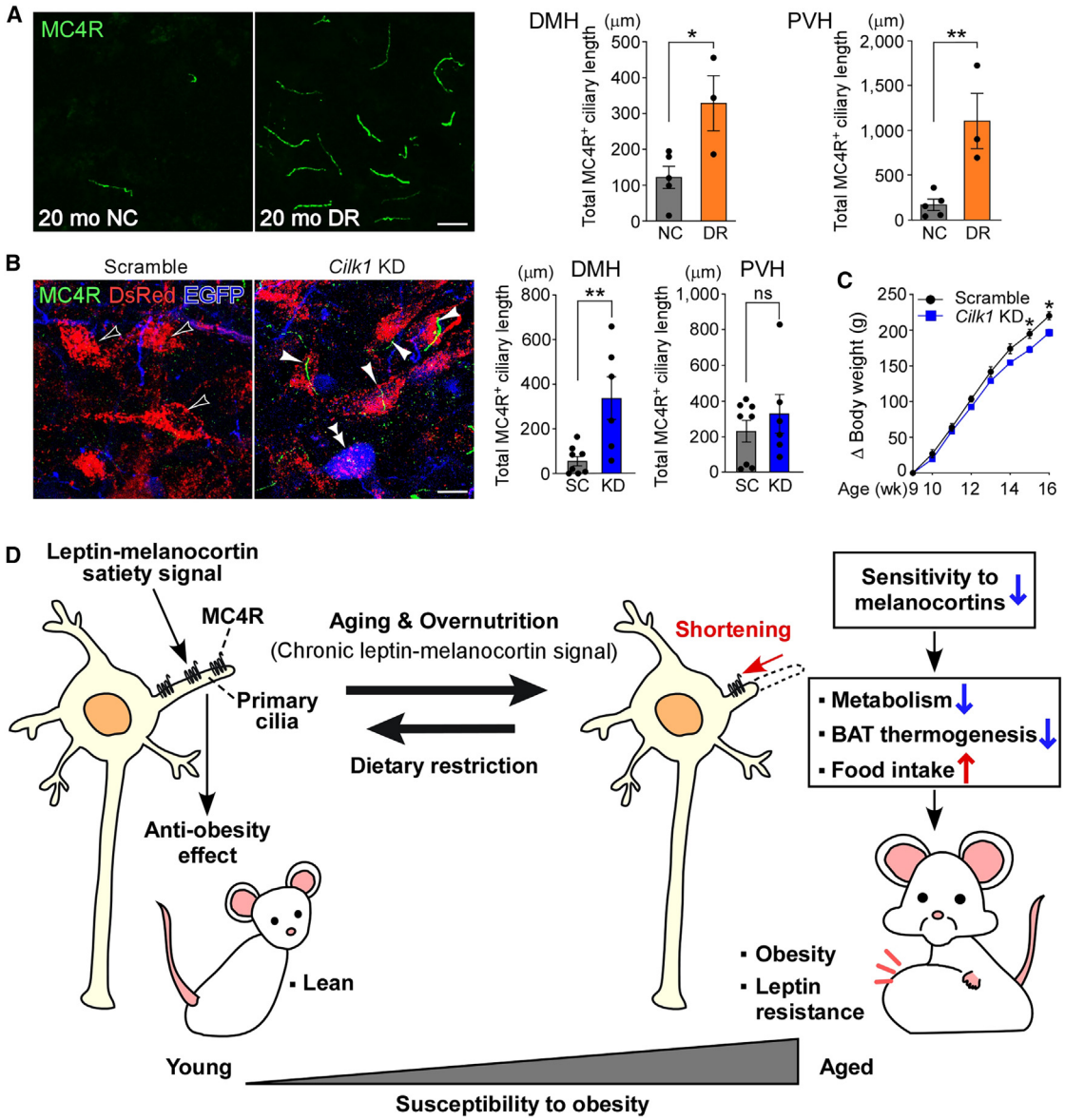

Figure 7. Interventions to prevent age-related shortening of MC4R$^+$ cilia

(A) DR regenerates MC4R$^+$ cilia in old rats. Left: MC4R-immunoreactive cilia in the DMH of 20-month-old wild-type rats fed NC *ad libitum* or after 8 weeks of DR. Scale bars, 10 μm. Right: length of MC4R-immunoreactive cilia is compared between NC (n = 5) and DR (n = 3) rats (unpaired t test, *p < 0.05 and **p < 0.01).

(B and C) Molecular intervention to prevent the age-related shortening of MC4R$^+$ cilia. Scramble AAV or AAV-dsRed-pSico-*Cilk1* shRNA (*Cilk1* KD) was bilaterally injected into the DMH and PVH of 9-week-old *Mc4r*-Cre rats, which were then *ad libitum* fed HFD for 7 weeks. Pseudocolored confocal images in the DMH 7 weeks after AAV injection (B) show that *Mc4r*-Cre-positive neurons, labeled with dsRed only (single arrowheads), lost MC4R-immunoreactive cilia due to aging in scramble rats, but retained them in *Cilk1*-KD rats. Double arrowheads indicate an infected *Mc4r*-Cre-negative cell, which expressed both dsRed and EGFP. Scale bars, 10 μm. *Cilk1*-KD rats had longer MC4R-immunoreactive cilia in the DMH, but not in the PVH, than scramble rats (B, scramble, n = 8; *Cilk1* KD, n = 6, unpaired t test, **p < 0.01; ns, not significant). *Cilk1*-KD rats exhibited reduced body weight gain (C, two-way ANOVA followed by Bonferroni's post hoc test, *p < 0.05).

(D) A model for the mechanism of age-related obesity. MC4R$^+$ primary cilia of hypothalamic neurons progressively shorten with age. This "age-related ciliopathy" is promoted by overnutrition, which chronically sensitizes MC4Rs to melanocortins, whereas it is inhibited by dietary restriction. The shortening of MC4R$^+$ cilia impairs neuronal sensitivity to leptin-melanocortin satiety signals, thereby decreasing metabolism and BAT thermogenesis, increasing food intake, and ultimately developing obesity and leptin resistance.

observation of the ciliary localization of GFP-tagged MC4Rs in PVH neurons in a genetically engineered mouse model.[14] Remarkably, MC4R$^+$ cilia shorten with age after peaking at 3 weeks old, the average weaning age for rats. The shortening of MC4R$^+$ cilia in the DMH correlated with the post-weaning, age-related reduction in energy expenditure and with the accompanying increase in adiposity. Our *in vivo* experiments in *Mc4r*-Cre knockin rats showed that the *Ift88* KD-mediated

selective shortening of MC4R$^+$ cilia in both DMH and PVH neurons of 9-week-old rats, which otherwise still have substantial MC4R$^+$ cilia, increased body weight and adiposity by reducing energy expenditure and increasing food intake. The shortening of MC4R$^+$ cilia also developed leptin resistance. These findings indicate that the length of MC4R$^+$ primary cilia of DMH and PVH neurons is a strong determinant of the sensitivity to leptin-melanocortin satiety signaling in the central regulation of systemic energy balance; therefore, the age-related shortening of these cilia predisposes to obesity by reducing energy expenditure and increasing food intake via a reduction in the sensitivity to leptin-melanocortin signaling (Figure 7D).

The age-related shortening of MC4R$^+$ primary cilia was facilitated by overnutrition but inhibited by undernutrition (DR). However, the age-related shortening of MC4R$^+$ cilia was inhibited by impaired leptin signaling in Zucker *fa/fa* obese rats and promoted by chronic leptin injection. Our data indicate that leptin-melanocortin signaling, which is augmented by increased adiposity after chronic overnutrition, facilitates the shortening of MC4R$^+$ cilia. Therefore, although leptin-melanocortin signaling acutely elicits anti-obesity responses via MC4Rs, it chronically promotes the age-related shortening of MC4R$^+$ primary cilia, thereby reducing the sensitivity to the satiety signaling itself to increase susceptibility to obesity (Figure 7D). MC4Rs are coupled to the G_s-AC pathway to increase intracellular cAMP levels.[32,33] We found that the constitutive activation of AC3 in MC4R-expressing DMH neurons eliminates their MC4R$^+$ cilia. Although *in vitro* studies have yielded inconsistent results regarding the effect of increased cAMP on ciliary length,[39,40] our *in vivo* data suggest the presence of a cAMP-mediated mechanism that shortens MC4R$^+$ primary cilia in hypothalamic neurons.

The present *Ift88* KD selectively shortened MC4R$^+$ cilia in the specific hypothalamic regions, DMH and PVH. The *Ift88* KD-mediated shortening of MC4R$^+$ cilia in both DMH and PVH neurons increased food intake and decreased energy expenditure. In contrast, the shortening of MC4R$^+$ cilia only in DMH neurons had no effect on food intake but decreased energy expenditure. Furthermore, the loss of MC4R$^+$ cilia only in PVH neurons was sufficient to develop leptin resistance in feeding regulation, and MC4R$^+$-ciliated PVH neurons contained OXT and TRH, which suppress appetite.[41,42] These findings are consistent with the view that MC4Rs in the DMH and PVH mediate different melanocortin effects, increasing energy expenditure and decreasing food intake, respectively.[43,44]

We further demonstrate that BAT is an important metabolic effector for the increase in energy expenditure by MC4Rs in the DMH. Our physiological and anatomical results show that MC4Rs on primary cilia of DMH neurons stimulate BAT thermogenesis via the innervation of sympathetic premotor neurons in the rMR and that the shortening of MC4R$^+$ cilia in DMH neurons blunts cooling- and MTII-evoked BAT thermogenesis. The post-weaning shortening of MC4R$^+$ primary cilia in the DMH correlated with age-related reduction in oxygen consumption, and the artificial (*Ift88* KD) shortening of MC4R$^+$ cilia in the DMH increased adiposity and body weight gain. Therefore, BAT thermogenesis stimulated by MC4R-mediated melanocortin signaling in the DMH substantially contributes to the anti-obesity effect of melanocortins, and the post-weaning shortening of MC4R$^+$ cilia of DMH neurons leads to an age-related decline in BAT thermogenesis, which has been linked to the development of obesity in middle-aged humans.[3]

BAT thermogenesis is also important for cold defense, especially in pups. Therefore, it seems reasonable that MC4R$^+$ cilia of DMH neurons are longest around the time of weaning. During the lactation period, pups manage to maintain body temperature by receiving body heat from their dam, but soon after weaning, they need to produce sufficient amounts of heat on their own by activating BAT and other metabolic thermogenesis, which is probably boosted by the MC4R-mediated sensitization of sympathoexcitatory DMH neurons. However, the rate of heat production required to maintain body temperature decreases with development, as the heat loss per body weight decreases due to the reduction in the body-surface area-to-mass ratio. Therefore, the post-weaning shortening of MC4R$^+$ cilia of DMH neurons, which leads to the age-related decline in BAT thermogenesis, may in part be an adaptation process for thermal homeostasis during the increase in body mass. In adults, the shortened MC4R$^+$ cilia of DMH and PVH neurons, which keep energy expenditure low and appetite high, confer the resistance to starvation, which mammals have experienced throughout evolution. However, this mechanism increases the susceptibility to obesity in food-satiated animals, perhaps including modern humans.

Leptin therapy was initially expected to have the same success in treating people with obesity as insulin has had in treating patients with diabetes.[45] However, a major problem is that most patients with obesity have elevated plasma leptin levels and would be resistant to exogenous leptin.[29,46] Although the etiology of hyperleptinemia and leptin resistance is unknown, rodent studies have shown that the cellular response to leptin (e.g., the activation of intracellular signal transducer and activator of transcription 3 [STAT3] signaling) in the arcuate nucleus is preserved in diet-induced obese, hyperleptinemic animals,[47] suggesting that the cause of leptin resistance is downstream of arcuate nucleus neurons sensitized by leptin. Our results suggest that the loss of MC4R$^+$ primary cilia of hypothalamic neurons due to chronic sensitization to leptin-melanocortin signaling may be a major cause of leptin resistance in patients with obesity. Supporting this view, chronic hyperleptinemia is required for the development of leptin resistance in mice.[48]

Importantly, we found that DR inhibits the age-related shortening of MC4R$^+$ cilia and even regenerates MC4R$^+$ cilia once they are diminished due to aging. Therefore, DR is likely to be an effective way to treat patients with obesity because it not only expends excess energy stored in fat tissues but also restores sensitivity to leptin-melanocortin signals. The effect of DR on MC4R$^+$ ciliary length may be due not only to decreased melanocortinergic satiety signaling but also to increased hunger signaling mediated by agouti-related protein (AgRP), an endogenous MC4R antagonist released by arcuate nucleus neurons. Our results also suggest that the severe obesity in the hereditary ciliopathies Bardet-Biedl syndrome and Alström syndrome[49,50] is ascribable to diminished MC4R$^+$ cilia of hypothalamic neurons. MC4R agonists may still be effective in treating patients with these and other types of obesity[51] via hypothalamic MC4Rs on remnant cilia in the patients, but

the effect may wane if chronic administration eliminates MC4R$^+$ cilia in humans. Molecular intervention in the intraflagellar transport machinery, as shown in our *Cilk1* KD study, may be a potential approach to enhance the neuronal sensitivity to MC4R agonists.

Limitations of the study

The present immunohistochemistry visualized the localization of MC4R proteins in primary cilia of hypothalamic neurons. However, this observation does not exclude the possibility that MC4R proteins are present at subdetectable levels in other subcellular parts of neurons or other brain regions. Moreover, most of the present analyses were performed in male rats because the age-related shortening of MC4R$^+$ cilia was similar in both sexes. On the other hand, sex differences are known in several aspects of obesity and the regulation of energy homeostasis in rodents and humans.[52] Therefore, further studies are needed to address how the age-related shortening of MC4R$^+$ cilia contributes to obesity in females, especially in association with female-specific events, such as pregnancy. The differences between rodents and humans, such as lifespan, should also be considered when interpreting the present findings. The age-related shortening of MC4R$^+$ cilia in the human hypothalamus needs to be investigated.

STAR★METHODS

Detailed methods are provided in the online version of this paper and include the following:

- KEY RESOURCES TABLE
- RESOURCE AVAILABILITY
  - Lead contact
  - Materials availability
  - Data and code availability
- EXPERIMENTAL MODELS AND SUBJECT DETAILS
  - Generation of *Mc4r*-T2A-iCre knockin rats
  - Animals
- METHOD DETAILS
  - AAV vectors
  - Stereotaxic injection into the brain
  - Development of anti-MC4R antibodies
  - DNA transfection into cultured cells and MC4R immunocytochemistry
  - Immunohistochemistry
  - *In situ* hybridization combined with immunohistochemistry
  - Measurement of ciliary length
  - Measurements of body fat percentage, metabolism, and body surface area
  - Measurement of food intake and dietary restriction
  - Leptin resistance test
  - Chronic leptin injection
  - Measurement of serum leptin
  - Quantitative real-time PCR
  - Telemetry
  - *In vivo* physiological experiment
- QUANTIFICATION AND STATICAL ANALYSIS
  - Anatomy and statistical analysis

SUPPLEMENTAL INFORMATION

Supplemental information can be found online at https://doi.org/10.1016/j.cmet.2024.02.010.

ACKNOWLEDGMENTS

We thank Misako Takemoto for technical assistance in AAV production and genotyping, Kosuke Hattori for technical assistance in the production of *Mc4r*-T2A-iCre knockin rats, Ronald S. Duman for sharing pAAV-dsRed-pSico, Joel K. Elmquist for sharing *Mc4r*-deficient mice, Csaba Fekete for sharing anti-TRH serum, Hiroyuki Hioki for sharing VGLUT3 and mRFP antibodies, and Shiki Okamoto and Hiroshi Suzuki for helpful advice on shRNA experiments. The maintenance of the *Mc4r*-T2A-iCre knockin rat strain was supported by the Center for Animal Research and Education, Nagoya University. Histological experiments were partly supported by the Division for Medical Research Engineering, Nagoya University Graduate School of Medicine. This study was supported by the AMED Project for Elucidating and Controlling Mechanisms of Aging and Longevity (JP21gm5010002 to K.N.), JST Moonshot R&D (JPMJMS2023 to K.N.), AMED-CREST (JP23gm1910003 to K.N.), and MEXT/JSPS KAKENHI (JP21K15343 and JP17K15571 to M.O.; JP21K06767 to Y.N.; and JP23H00398, JP20H03418, JP16H06276 [AdAMS], and JP15H05932 to K.N.). M.O. was supported by the JSPS Research Fellowship for Young Scientists (RPD).

AUTHOR CONTRIBUTIONS

K.N. conceived the research. M.O., Y.N., and K.N. designed and performed experiments. K.N. developed anti-MC4R antibodies. Y.M. and T.M. generated *Mc4r*-Cre knockin rats. M.T. and T.S. provided *Mc4r*-deficient mice. M.O., Y.N., M.T., T.S., and K.N. discussed data. M.O. and K.N. wrote the manuscript with input from all authors. All authors approved the manuscript.

DECLARATION OF INTERESTS

The authors declare no competing interests.

Received: July 30, 2023
Revised: January 16, 2024
Accepted: February 15, 2024
Published: March 6, 2024

REFERENCES

1. St-Onge, M.P., and Gallagher, D. (2010). Body composition changes with aging: the cause or the result of alterations in metabolic rate and macronutrient oxidation? Nutrition *26*, 152–155.
2. Volpi, E., Nazemi, R., and Fujita, S. (2004). Muscle tissue changes with aging. Curr. Opin. Clin. Nutr. Metab. Care *7*, 405–410.
3. Yoneshiro, T., Aita, S., Matsushita, M., Okamatsu-Ogura, Y., Kameya, T., Kawai, Y., Miyagawa, M., Tsujisaki, M., and Saito, M. (2011). Age-related decrease in cold-activated brown adipose tissue and accumulation of body fat in healthy humans. Obesity (Silver Spring) *19*, 1755–1760.
4. Nakamura, K., Nakamura, Y., and Kataoka, N. (2022). A hypothalamomedullary network for physiological responses to environmental stresses. Nat. Rev. Neurosci. *23*, 35–52.
5. Kim, D., Hou, W., Wang, F., and Arcan, C. (2019). Factors affecting obesity and waist circumference among US adults. Prev. Chronic Dis. *16*, 180220.
6. Kishi, T., Aschkenasi, C.J., Lee, C.E., Mountjoy, K.G., Saper, C.B., and Elmquist, J.K. (2003). Expression of melanocortin 4 receptor mRNA in the central nervous system of the rat. J. Comp. Neurol. *457*, 213–235.
7. Spiegelman, B.M., and Flier, J.S. (2001). Obesity and the regulation of energy balance. Cell *104*, 531–543.
8. Barsh, G.S., and Schwartz, M.W. (2002). Genetic approaches to studying energy balance: perception and integration. Nat. Rev. Genet. *3*, 589–600.
9. Cone, R.D. (2006). Studies on the physiological functions of the melanocortin system. Endocr. Rev. *27*, 736–749.

10. Ahima, R.S., and Flier, J.S. (2000). Leptin. Annu. Rev. Physiol. *62*, 413–437.

11. Huszar, D., Lynch, C.A., Fairchild-Huntress, V., Dunmore, J.H., Fang, Q., Berkemeier, L.R., Gu, W., Kesterson, R.A., Boston, B.A., Cone, R.D., et al. (1997). Targeted disruption of the melanocortin-4 receptor results in obesity in mice. Cell *88*, 131–141.

12. Yeo, G.S., Farooqi, I.S., Aminian, S., Halsall, D.J., Stanhope, R.G., and O'Rahilly, S. (1998). A frameshift mutation in MC4R associated with dominantly inherited human obesity. Nat. Genet. *20*, 111–112.

13. Garza, J.C., Kim, C.S., Liu, J., Zhang, W., and Lu, X.Y. (2008). Adeno-associated virus-mediated knockdown of melanocortin-4 receptor in the paraventricular nucleus of the hypothalamus promotes high-fat diet-induced hyperphagia and obesity. J. Endocrinol. *197*, 471–482.

14. Siljee, J.E., Wang, Y., Bernard, A.A., Ersoy, B.A., Zhang, S., Marley, A., Von Zastrow, M., Reiter, J.F., and Vaisse, C. (2018). Subcellular localization of MC4R with ADCY3 at neuronal primary cilia underlies a common pathway for genetic predisposition to obesity. Nat. Genet. *50*, 180–185.

15. Millar, W.J., and Stephens, T. (1987). The prevalence of overweight and obesity in Britain, Canada, and United States. Am. J. Public Health *77*, 38–41.

16. Grundy, S.M. (2008). Metabolic syndrome pandemic. Arterioscler. Thromb. Vasc. Biol. *28*, 629–636.

17. Singla, V., and Reiter, J.F. (2006). The primary cilium as the cell's antenna: signaling at a sensory organelle. Science *313*, 629–633.

18. Liu, H., Kishi, T., Roseberry, A.G., Cai, X., Lee, C.E., Montez, J.M., Friedman, J.M., and Elmquist, J.K. (2003). Transgenic mice expressing green fluorescent protein under the control of the melanocortin-4 receptor promoter. J. Neurosci. *23*, 7143–7154.

19. Nakamura, Y., Yahiro, T., Fukushima, A., Kataoka, N., Hioki, H., and Nakamura, K. (2022). Prostaglandin EP3 receptor-expressing preoptic neurons bidirectionally control body temperature via tonic GABAergic signaling. Sci. Adv. *8*, eadd5463.

20. Kataoka, N., Hioki, H., Kaneko, T., and Nakamura, K. (2014). Psychological stress activates a dorsomedial hypothalamus-medullary raphe circuit driving brown adipose tissue thermogenesis and hyperthermia. Cell Metab. *20*, 346–358.

21. Nakamura, K., Matsumura, K., Hübschle, T., Nakamura, Y., Hioki, H., Fujiyama, F., Boldogköi, Z., König, M., Thiel, H.J., Gerstberger, R., et al. (2004). Identification of sympathetic premotor neurons in medullary raphe regions mediating fever and other thermoregulatory functions. J. Neurosci. *24*, 5370–5380.

22. Wohleb, E.S., Wu, M., Gerhard, D.M., Taylor, S.R., Picciotto, M.R., Alreja, M., and Duman, R.S. (2016). GABA interneurons mediate the rapid antidepressant-like effects of scopolamine. J. Clin. Invest. *126*, 2482–2494.

23. Moriyoshi, K., Richards, L.J., Akazawa, C., O'Leary, D.D.M., and Nakanishi, S. (1996). Labeling neural cells using adenoviral gene transfer of membrane-targeted GFP. Neuron *16*, 255–260.

24. Chen, X.M., Nishi, M., Taniguchi, A., Nagashima, K., Shibata, M., and Kanosue, K. (2002). The caudal periaqueductal gray participates in the activation of brown adipose tissue in rats. Neurosci. Lett. *331*, 17–20.

25. Schneeberger, M., Parolari, L., Das Banerjee, T., Bhave, V., Wang, P., Patel, B., Topilko, T., Wu, Z., Choi, C.H.J., Yu, X., et al. (2019). Regulation of energy expenditure by brainstem GABA neurons. Cell *178*, 672–685.e12.

26. Tu, H.Q., Li, S., Xu, Y.L., Zhang, Y.C., Li, P.Y., Liang, L.Y., Song, G.P., Jian, X.X., Wu, M., Song, Z.Q., et al. (2023). Rhythmic cilia changes support SCN neuron coherence in circadian clock. Science *380*, 972–979.

27. Pazour, G.J., Dickert, B.L., Vucica, Y., Seeley, E.S., Rosenbaum, J.L., Witman, G.B., and Cole, D.G. (2000). Chlamydomonas IFT88 and its mouse homologue, polycystic kidney disease gene tg737, are required for assembly of cilia and flagella. J. Cell Biol. *151*, 709–718.

28. Clement, C.A., Kristensen, S.G., Møllgård, K., Pazour, G.J., Yoder, B.K., Larsen, L.A., and Christensen, S.T. (2009). The primary cilium coordinates early cardiogenesis and hedgehog signaling in cardiomyocyte differentiation. J. Cell Sci. *122*, 3070–3082.

29. Friedman, J.M. (2019). Leptin and the endocrine control of energy balance. Nat. Metab. *1*, 754–764.

30. Myers, M.G., Jr., Leibel, R.L., Seeley, R.J., and Schwartz, M.W. (2010). Obesity and leptin resistance: distinguishing cause from effect. Trends Endocrinol. Metab. *21*, 643–651.

31. Yamashita, T., Murakami, T., Iida, M., Kuwajima, M., and Shima, K. (1997). Leptin receptor of Zucker fatty rat performs reduced signal transduction. Diabetes *46*, 1077–1080.

32. Gantz, I., Miwa, H., Konda, Y., Shimoto, Y., Tashiro, T., Watson, S.J., DelValle, J., and Yamada, T. (1993). Molecular cloning, expression, and gene localization of a fourth melanocortin receptor. J. Biol. Chem. *268*, 15174–15179.

33. Mountjoy, K.G., Mortrud, M.T., Low, M.J., Simerly, R.B., and Cone, R.D. (1994). Localization of the melanocortin-4 receptor (MC4-R) in neuroendocrine and autonomic control circuits in the brain. Mol. Endocrinol. *8*, 1298–1308.

34. Pitman, J.L., Wheeler, M.C., Lloyd, D.J., Walker, J.R., Glynne, R.J., and Gekakis, N. (2014). A gain-of-function mutation in adenylate cyclase 3 protects mice from diet-induced obesity. PLoS One *9*, e110226.

35. Wang, W., Jack, B.M., Wang, H.H., Kavanaugh, M.A., Maser, R.L., and Tran, P.V. (2021). Intraflagellar transport proteins as regulators of primary cilia length. Front. Cell Dev. Biol. *9*, 661350.

36. Moon, H., Song, J., Shin, J.O., Lee, H., Kim, H.K., Eggenschwiller, J.T., Bok, J., and Ko, H.W. (2014). Intestinal cell kinase, a protein associated with endocrine-cerebro-osteodysplasia syndrome, is a key regulator of cilia length and Hedgehog signaling. Proc. Natl. Acad. Sci. USA *111*, 8541–8546.

37. Broekhuis, J.R., Verhey, K.J., and Jansen, G. (2014). Regulation of cilium length and intraflagellar transport by the RCK-kinases ICK and MOK in renal epithelial cells. PLoS One *9*, e108470.

38. Ma, R., Kutchy, N.A., Chen, L., Meigs, D.D., and Hu, G. (2022). Primary cilia and ciliary signaling pathways in aging and age-related brain disorders. Neurobiol. Dis. *163*, 105607.

39. Besschetnova, T.Y., Kolpakova-Hart, E., Guan, Y., Zhou, J., Olsen, B.R., and Shah, J.V. (2010). Identification of signaling pathways regulating primary cilium length and flow-mediated adaptation. Curr. Biol. *20*, 182–187.

40. Porpora, M., Sauchella, S., Rinaldi, L., Delle Donne, R., Sepe, M., Torres-Quesada, O., Intartaglia, D., Garbi, C., Insabato, L., Santoriello, M., et al. (2018). Counterregulation of cAMP-directed kinase activities controls ciliogenesis. Nat. Commun. *9*, 1224.

41. Arletti, R., Benelli, A., and Bertolini, A. (1989). Influence of oxytocin on feeding behavior in the rat. Peptides *10*, 89–93.

42. Morley, J.E., and Levine, A.S. (1980). Thyrotropin releasing hormone (TRH) suppresses stress induced eating. Life Sci. *27*, 269–274.

43. Balthasar, N., Dalgaard, L.T., Lee, C.E., Yu, J., Funahashi, H., Williams, T., Ferreira, M., Tang, V., McGovern, R.A., Kenny, C.D., et al. (2005). Divergence of melanocortin pathways in the control of food intake and energy expenditure. Cell *123*, 493–505.

44. Chen, M., Shrestha, Y.B., Podyma, B., Cui, Z., Naglieri, B., Sun, H., Ho, T., Wilson, E.A., Li, Y.Q., Gavrilova, O., and Weinstein, L.S. (2017). Gsα deficiency in the dorsomedial hypothalamus underlies obesity associated with Gsα mutations. J. Clin. Invest. *127*, 500–510.

45. Flier, J.S. (2019). Starvation in the midst of plenty: reflections on the history and biology of insulin and leptin. Endocr. Rev. *40*, 1–16.

46. Schwartz, M.W., Seeley, R.J., Zeltser, L.M., Drewnowski, A., Ravussin, E., Redman, L.M., and Leibel, R.L. (2017). Obesity pathogenesis: an Endocrine Society scientific statement. Endocr. Rev. *38*, 267–296.

47. Ottaway, N., Mahbod, P., Rivero, B., Norman, L.A., Gertler, A., D'Alessio, D.A., and Perez-Tilve, D. (2015). Diet-induced obese mice retain endogenous leptin action. Cell Metab. *21*, 877–882.

48. Knight, Z.A., Hannan, K.S., Greenberg, M.L., and Friedman, J.M. (2010). Hyperleptinemia is required for the development of leptin resistance. PLoS One *5*, e11376.

49. Girard, D., and Petrovsky, N. (2011). Alström syndrome: insights into the pathogenesis of metabolic disorders. Nat. Rev. Endocrinol. *7*, 77–88.

50. Forsythe, E., and Beales, P.L. (2013). Bardet–Biedl syndrome. Eur. J. Hum. Genet. *21*, 8–13.

51. Haqq, A.M., Chung, W.K., Dollfus, H., Haws, R.M., Martos-Moreno, G.Á., Poitou, C., Yanovski, J.A., Mittleman, R.S., Yuan, G., Forsythe, E., et al. (2022). Efficacy and safety of setmelanotide, a melanocortin-4 receptor agonist, in patients with Bardet-Biedl syndrome and Alström syndrome: a multicentre, randomised, double-blind, placebo-controlled, phase 3 trial with an open-label period. Lancet Diabetes Endocrinol. *10*, 859–868.

52. Lovejoy, J.C., and Sainsbury, A.; Stock Conference 2008 Working Group (2009). Sex differences in obesity and the regulation of energy homeostasis. Obes. Rev. *10*, 154–167.

53. Hioki, H., Fujiyama, F., Nakamura, K., Wu, S.X., Matsuda, W., and Kaneko, T. (2004). Chemically specific circuit composed of vesicular glutamate transporter 3- and preprotachykinin B-producing interneurons in the rat neocortex. Cereb. Cortex *14*, 1266–1275.

54. Wittmann, G., Füzesi, T., Liposits, Z., Lechan, R.M., and Fekete, C. (2009). Distribution and axonal projections of neurons coexpressing thyrotropin-releasing hormone and urocortin 3 in the rat brain. J. Comp. Neurol. *517*, 825–840.

55. Hioki, H., Nakamura, H., Ma, Y.F., Konno, M., Hayakawa, T., Nakamura, K.C., Fujiyama, F., and Kaneko, T. (2010). Vesicular glutamate transporter 3-expressing nonserotonergic projection neurons constitute a subregion in the rat midbrain raphe nuclei. J. Comp. Neurol. *518*, 668–686.

56. Kataoka, N., Shima, Y., Nakajima, K., and Nakamura, K. (2020). A central master driver of psychosocial stress responses in the rat. Science *367*, 1105–1112.

57. Yoshimi, K., Kunihiro, Y., Kaneko, T., Nagahora, H., Voigt, B., and Mashimo, T. (2016). ssODN-mediated knock-in with CRISPR-Cas for large genomic regions in zygotes. Nat. Commun. *7*, 10431.

58. van Gestel, M.A., van Erp, S., Sanders, L.E., Brans, M.A.D., Luijendijk, M.C.M., Merkestein, M., Pasterkamp, R.J., and Adan, R.A.H. (2014). shRNA-induced saturation of the microRNA pathway in the rat brain. Gene Ther. *21*, 205–211.

59. Takahashi, M., Ishida, Y., Kataoka, N., Nakamura, K., and Hioki, H. (2021). Efficient labeling of neurons and identification of postsynaptic sites using adeno-associated virus vector. Receptor and Ion Channel Detection in the Brain. Neuromethods, 169. Humana. pp. 323–341.

60. Nakamura, K., Kaneko, T., Yamashita, Y., Hasegawa, H., Katoh, H., and Negishi, M. (2000). Immunohistochemical localization of prostaglandin EP3 receptor in the rat nervous system. J. Comp. Neurol. *421*, 543–569.

61. Wang, F., Flanagan, J., Su, N., Wang, L.C., Bui, S., Nielson, A., Wu, X., Vo, H.T., Ma, X.J., and Luo, Y. (2012). RNAscope: a novel in situ RNA analysis platform for formalin-fixed, paraffin-embedded tissues. J. Mol. Diagn. *14*, 22–29.

62. Gouma, E., Simos, Y., Verginadis, I., Lykoudis, E., Evangelou, A., and Karkabounas, S. (2012). A simple procedure for estimation of total body surface area and determination of a new value of Meeh's constant in rats. Lab. Anim. *46*, 40–45.

63. Lecklin, A., Hermonen, P., Tarhanen, J., and Männistö, P.T. (2000). An acute i.c.v. infusion of leptin has no effect on hypothalamic histamine and tele-methylhistamine contents in Wistar rats. Eur. J. Pharmacol. *395*, 113–119.

64. Nakamura, K., and Morrison, S.F. (2007). Central efferent pathways mediating skin cooling-evoked sympathetic thermogenesis in brown adipose tissue. Am. J. Physiol. Regul. Integr. Comp. Physiol. *292*, R127–R136.

65. Nakamura, K., and Morrison, S.F. (2011). Central efferent pathways for cold-defensive and febrile shivering. J. Physiol. *589*, 3641–3658.

66. Paxinos, G., and Watson, C. (2007). The Rat Brain in Stereotaxic Coordinates, Sixth Edition (Academic Press).

67. Watts, A.G. (2015). 60 years of neuroendocrinology: the structure of the neuroendocrine hypothalamus: the neuroanatomical legacy of Geoffrey Harris. J. Endocrinol. *226*, T25–T39.

68. Nakamura, K., Matsumura, K., Kaneko, T., Kobayashi, S., Katoh, H., and Negishi, M. (2002). The rostral raphe pallidus nucleus mediates pyrogenic transmission from the preoptic area. J. Neurosci. *22*, 4600–4610.

STAR★METHODS

KEY RESOURCES TABLE

REAGENT or RESOURCE	SOURCE	IDENTIFIER
Antibodies		
Guinea pig anti-MC4R N-terminal antibody	This paper	N/A
Guinea pig anti-MC4R C-terminal antibody	This paper	N/A
Guinea pig anti-VGLUT3 antibody	Hioki et al.[53]	RRID: AB_2336888
Mouse anti-GFP antibody	Thermo Fisher Scientific	Cat # A-11120; RRID: AB_221568
Rabbit anti-AC3 antibody	Santa Cruz Biotechnology	Cat # sc-588; RRID: AB_630839
Rabbit anti-OXT serum	Immunostar	Cat # 20068; RRID: AB_572258
Rabbit anti-AVP serum	Merck	Cat # PC234L; RRID: AB_565256
Sheep anti-α-MSH serum	Merck	Cat # AB5087; RRID: AB_91683
Rabbit anti-CRH serum	Peninsula Laboratories	Cat # T-4037; RRID: AB_518252
Sheep anti-TRH serum	Wittmann et al.[54]	RRID: AB_2315482
Rabbit anti-IFT88 antibody	Proteintech	Cat # 13967-1-AP; RRID: AB_2121979
Rabbit anti-mRFP antibody	Hioki et al.[55]	RRID: AB_2336889
Alexa488-conjugated goat antibody to guinea pig IgG	Thermo Fisher Scientific	Cat # A-11073; RRID: AB_2534117
Alexa647-conjugated goat antibody to guinea pig IgG	Thermo Fisher Scientific	Cat # A-21450; RRID: AB_141882
Alexa594-conjugated goat antibody to guinea pig IgG	Thermo Fisher Scientific	Cat # A-11076; RRID: AB_141930
Alexa594-conjugated goat antibody to rabbit IgG	Thermo Fisher Scientific	Cat # A-11037; RRID: AB_2534095
Alexa488-conjugated goat antibody to rabbit IgG	Thermo Fisher Scientific	Cat # A-11034; RRID: AB_2576217
Alexa488-conjugated donkey antibody to goat IgG	Thermo Fisher Scientific	Cat # A-11055; RRID: AB_2534102
Alexa488-conjugated goat antibody to mouse IgG	Thermo Fisher Scientific	Cat # A-11029; RRID: AB_2534088
Alexa647-conjugated goat antibody to rabbit IgG	Thermo Fisher Scientific	Cat # A-21245; RRID: AB_2535813
Biotinylated donkey antibody to guinea pig IgG	Jackson ImmunoResearch	Cat # 706-065-148; RRID: AB_2340451
Biotinylated donkey antibody to mouse IgG	Merck	Cat # AP192B; RRID: AB_92624
Biotinylated donkey antibody to rabbit IgG	Merck	Cat # AP182B; RRID: AB_92587
Biotinylated donkey antibody to goat IgG	Merck	Cat # AP180B; RRID: AB_92569
Bacterial and virus strains		
AAV2/1-EF1α-DIO-palGFP	Kataoka et al.[56]	N/A
AAV2/1-dsRed-pSico-scramble	This paper	N/A
AAV2/1-dsRed-pSico-*Ift88* shRNA	This paper	N/A
AAV2/1-dsRed-pSico-*Cilk1* shRNA	This paper	N/A
AAV2/1-U6-GFP-scramble	This paper	N/A
AAV2/1-U6-GFP-*Ift88* shRNA #1	This paper	N/A
AAV2/1-U6-GFP-*Ift88* shRNA #2	This paper	N/A
Chemicals, peptides, and recombinant proteins		
Nt.BspQI, Nb.BbvCI	New England Biolabs	R0644, R0631
Pregnant mare serum gonadotropin	ASKA Animal Health	N/A
Human chorionic gonadotropin	ASKA Animal Health	N/A
Rat KSOM medium	ARK Resource	Cat # Rat KSOM
Opti-MEM	Thermo Fisher Scientific	Cat # 11058021 (500 mL liquid) and Cat # 22600050 (powder)
Standard pellet diet	Oriental Yeast	MF
MC4R N34 peptide (YTSLHLWNRSSHGL HGNASESLGKGHSDGGCYEQ)	Sigma-Aldrich	Custom made
MC4R C19 peptide (KEIICFYPLGGICELPGRY)	Sigma-Aldrich	Custom made
Maleimide-activated bovine serum albumin	Thermo Fisher Scientific	Cat # 77116
Freund's complete adjuvant	Difco	Cat # 263810

(*Continued on next page*)

Continued

REAGENT or RESOURCE	SOURCE	IDENTIFIER
SulfoLink Coupling Resin	Thermo Fisher Scientific	Cat # 20401
Lipofectamine 2000 transfection reagent	Thermo Fisher Scientific	Cat # 11668030
Avidin-biotinylated peroxidase complex	Vector Laboratories	Cat # PK-6100
3,3'-diaminobenzidine tetrahydrochloride	Merck	Cat # 281751
Avidin-biotin blocking kit	Vector Laboratories	Cat # SP-2001
Alexa594-conjugated CTb	Thermo Fisher Scientific	Cat # C34777
FITC-conjugated tyramide (Tyramide Signal Amplification FITC Systems)	Parkin Elmer	Cat # SAT701001KT
Alexa488-conjugated streptavidin	Thermo Fisher Scientific	Cat # S11223
Alexa594-conjugated streptavidin	Thermo Fisher Scientific	Cat # S11227
RNAscope negative control probe	Advanced Cell Diagnostics	Cat # 310043
RNAscope probe for *Cilk1*	Advanced Cell Diagnostics	Cat # 1177181-C1
Cy3-conjugated tyramide (TSA Plus Cyanine 3)	Akoya Biosciences	Cat # NEL744001KT
Food pellets for NC, HFD and DR rats	Research Diets	Cat # D12450H (NC) Cat # D12451 (HFD)
Pyrogen-free 0.9% saline	Otsuka	N/A
Recombinant rat leptin	R&D systems	Cat # 598-LP
RNAlater	Merck	N/A
MTII	Sigma-Aldrich	Cat # M8693
Fluorescent microbeads	Thermo Fisher Scientific	Cat # F8801, F8803
Critical commercial assays		
MEGAshortscript T7 Transcription Kit	Life Technologies	Cat # AM1354
mMESSAGE mMACHINE T7 Ultra Kit	Life Technologies	Cat # AM1345
MEGAClear kit	Life Technologies	Cat # AM1908
NucleoSpin Gel and PCR Clean-up	Takara Bio	Cat # 740609
KAPA Express Extract Kit	Kapa Biosystems	Cat # KK7100
RNAscope Multiplex Fluorescent Reagent Kit v2	Advanced Cell Diagnostics	Cat # 323100
Mouse/Rat Leptin Quantikine ELISA Kit	R&D Systems	Cat # MOB00B
RNeasy Lipid Tissue Mini Kit	Qiagen	Cat # 74804
iTaq Universal SYBR Green One-Step Kit	Bio-Rad	Cat # 1725150
Experimental models: Cell lines		
HEK293T	N/A	N/A
Experimental models: Organisms/strains		
Rat: Slc:Wistar/ST	Japan SLC	N/A
Rat: Iar:Wistar-Imamichi	Institute for Animal Reproduction	N/A
Rat: Slc:Zucker	Japan SLC	lean *Fa/fa* and obese *fa/fa*
Mc4r-deficient mice	Balthasar et al.[43]	N/A
Mouse: C57BL/6JJcl	CLEA Japan	N/A
Guinea pigs	Shimizu Experimental Materials	N/A
Oligonucleotides		
scrambled sequence (5'-GCGCTTAGCTGTAGGATTC TTCAAGAGAGAATCCTACAGCTAAGCGCTTTTTT-3')	Sigma-Aldrich	Custom made
Ift88 shRNA #1 (5'-GGCATTAGATACTTACAAATT CAAGAGATTTGTAAGTATCTAATGCCTTTTTT-3')	Sigma-Aldrich	Custom made
Ift88 shRNA #2 (5'-GTATTTCCCTTCTAACATTTTCA AGAGAAATGTTAGAAGGGAAATACTTTTTT-3')	Sigma-Aldrich	Custom made
Cilk1 shRNA (5'-CACAACCACGTGGCGGTGTAAT TCAAGAGATTACACCGCCACGTGGTTGTGTTTTTT-3')	Sigma-Aldrich	Custom made
Actb: forward 5'-CCACACTTTCTACAATGAGC-3' and reverse 5'-ATACAGGGACAACACAGC-3'	Thermo Fisher Scientific	Custom made

(*Continued on next page*)

Continued

REAGENT or RESOURCE	SOURCE	IDENTIFIER
Mc4r: forward 5'-GACGGAGGATGCTATGAG-3' and reverse 5'-AGGTTCTTGTTCTTGGCTAT-3'	Thermo Fisher Scientific	Custom made
Recombinant DNA		
pCas9-polyA	Addgene	Cat # 72602
pAAV2-CMV-Flex-Flag-*Adcy3*^{M279I}	Vector Builder	Custom made
pcDNA3	Invitrogen	N/A
Software and algorithms		
CRISPOR	http://crispor.tefor.net/	N/A
siDirect	http://sidirect2.rnai.jp	N/A
Imaris software version 9.6.0	Oxford Instruments	RRID: SCR_007370
Spike 2, version 7.10	CED	RRID: SCR_00903
Prism 7.04	GraphPad	RRID: SCR_002798
Other		
Gap electrode	Nepa Gene	Cat # CUY520P5
Electroporator (NEPA21 Super Electroporator)	Nepa Gene	Cat # Nepa21
DNA Sequencer (Applied Biosystems 3130*xl* Genetic Analyzer)	Thermo Fisher Scientific	3130xl-100
Epifluorescence microscope	Nikon	Eclipse 80i
Confocal laser-scanning microscope	Leica	TCS SP8
Body composition analyser	Hitachi	EchoMRI-900
Metabolism-measuring system	Muromachi Kikai	MK-5000RQ
3D scanner	Japan 3D printer	Einscan SP
Feedam	Melquest	cFDM-700AS
Microsyringe	Hamilton	N/A
Real-time PCR system	Thermo Fisher Scientific	StepOnePlus
Battery-operated telemetric transmitter	Data Science International	F40-TT
Telemetry system	Data Science International	PhysioTel and PONEMAH
Needle-type thermocouple	Physitemp	MT-29/2
Amplifier for electrophysiological recordings	Molecular Devices	CyberAmp 380
Picospritzer III	Parker	Cat # 052-0500-900

RESOURCE AVAILABILITY

Lead contact

Further information and requests for resources and reagents should be directed to and will be fulfilled by the lead contact, Kazuhiro Nakamura (kazu@med.nagoya-u.ac.jp).

Materials availability

Mc4r-T2A-iCre knockin rat, anti-MC4R antibody, and original AAVs are available from the lead contact under material transfer agreements.

Data and code availability

- Data S1. Unprocessed data underlying the display items in the manuscript, related to Figures 1, 2, 3, 4, 5, 6, 7, S2, and S4–S7.
- This paper does not report original code.
- Any additional information required to reanalyze the data reported in this paper is available from the lead contact upon request.

EXPERIMENTAL MODELS AND SUBJECT DETAILS

Generation of *Mc4r*-T2A-iCre knockin rats

Slc:Wistar/ST rats for the donor of embryos were obtained from Japan SLC (Shizuoka, Japan). Iar:Wistar-Imamichi rats for the transplant recipient of genome-edited zygotes were obtained from the Institute for Animal Reproduction (Ibaraki, Japan). To design the

guide RNA (gRNA) for the CRISPR-Cas9-mediated genome editing, we used the software tool CRISPOR (http://crispor.tefor.net/) to predict unique target sites throughout the rat genome. The target sequence selected for knock-in production was 5'-GTTACCTGG CAGGTATTAAG-3'. The gRNA was transcribed *in vitro* using a MEGAshortscript T7 Transcription Kit (Life Technologies, Carlsbad, CA) from synthetic double-stranded DNAs obtained from Integrated DNA Technologies (Coralville, IA). Cas9 mRNA was transcribed *in vitro* using a mMESSAGE mMACHINE T7 Ultra Kit (Life Technologies) from a linearized plasmid (pCas9-polyA; Addgene, #72602) and was purified using a MEGAClear kit (Life Technologies). As the knock-in donor, long single-stranded DNA (lssDNA) (Figure S2B) was prepared by a method using nicking endonucleases (nickase) as we reported.[57] Briefly, a double-stranded DNA plasmid containing homology arms, T2A sequence, iCre sequence, and two nicking endonuclease Nt.BspQI and Nb.BbvCI sites was custom-made by the GeneArt Gene Synthesis (Thermo Fisher Scientific). For digestion, 100 μg of the plasmid was incubated at an optimum temperature for 2–3 h with the two nicking endonucleases (New England Biolabs, MA). After ethanol precipitation, the DNAs were denatured with a 3-fold amount of formamide at 80°C for 10 min, and then applied to agarose gel electrophoresis. A band corresponding to a single-stranded DNA fragment was extracted using a NucleoSpin Gel and PCR Clean-up (Takara Bio, Shiga, Japan). Finally, 2–4 μg of lssDNA was obtained.

Pronuclear-stage rat embryos were collected from female Wistar/ST rats at 8–12 weeks old that were superovulated by an administration of 150 U/kg of pregnant mare serum gonadotropin (ASKA Animal Health, Tokyo, Japan) followed by 75 U/kg of human chorionic gonadotropin (ASKA Animal Health). After natural mating, pronuclear-stage embryos were collected from the oviducts of the females and cultured in a modified Krebs–Ringer bicarbonate medium or rat KSOM medium (ARK Resource, Kumamoto, Japan). For electroporation, 120 embryos at 3–4 h after collection were placed in a chamber with 40 μl of serum-free media (Opti-MEM, Thermo Fisher Scientific) containing 400 ng/μl Cas9 mRNA, 200 ng/μl gRNA, and 40 ng/μl lssDNA. They were then electroporated with a 5 mm gap electrode (CUY520P5, Nepa Gene, Chiba, Japan) in a NEPA21 Super Electroporator (Nepa Gene). The parameters of poring pulses for the electroporation were voltage 225 V, pulse width 2.0 ms, pulse interval 50 ms, and number of pulses 4. The parameters of transfer pulses were voltage 20 V, pulse width 50 ms, pulse interval 50 ms, and number of pulses 5. Total 72 of the 100 embryos that developed to the two-cell stage after the introduction of Cas9 mRNA, gRNA, and lssDNA were transferred into the oviducts of 3 female surrogates anesthetized with isoflurane. Finally, pups were born, and one of them was confirmed as a knock-in rat.

We performed genotyping and sequencing analyses with the primer sets (Figure S2B) to confirm the position and sequence of the inserted transgene in this knockin strain. Genomic DNA was extracted from the tail tips using the KAPA Express Extract Kit (Kapa Biosystems, London, UK). The PCR products amplified with specific primer sets were directly sequenced using a BigDye terminator v3.1 cycle sequencing mix according to the standard protocol for an Applied Biosystems 3130*xl* Genetic Analyzer (Life Technologies). The *Mc4r*-T2A-iCre knockin line was maintained in heterozygotes on a Wistar/ST genetic background, and transmission of the transgene to offsprings was monitored by PCR (Figure S2B).

Animals

Wistar rats (Slc:Wistar/ST) and Zucker rats (lean *Fa/fa*; 7 week old and obese *fa/fa*; 5 week old) were purchased from Japan SLC. *Mc4r*-deficient mice on the C57BL/6J background were a gift from Dr. Joel K. Elmquist (University of Texas Southwestern Medical Center).[43] C57BL/6J wild-type mice were purchased from CLEA Japan (Tokyo, Japan). Rats and mice used in experiments were male, except in Figure S4G, which used female rats. All rats and mice were two or three to a cage with *ad libitum* access to a standard pellet diet (MF, Oriental Yeast, Tokyo, Japan) and water in a room air-conditioned at 25 ± 2°C under a 12 h light/dark cycle (lights on from 7:00 a.m. to 7:00 p.m.) until being used for experiments or surgery. Animals were randomly allocated to each experimental group. Male and female guinea pigs (200–250 g) for the production of anti-MC4R antibodies were purchased from Shimizu Experimental Materials (Kyoto, Japan). All procedures conform to the guidelines of animal care by the Division of Experimental Animals, Nagoya University Graduate School of Medicine and by the Institute of Laboratory Animals, Faculty of Medicine, Kyoto University, and were approved by the Nagoya University Animal Experiment Committee (approval #M220097-002) and the Animal Research Committee of Osaka University (approval #24-006-042).

METHOD DETAILS

AAV vectors

The recombinant AAVs used in the present study were serotype 1. The production of AAV-EF1α-DIO-palGFP was reported previously.[56] For production of AAV-dsRed-pSico-scramble, AAV-dsRed-pSico-*Ift88* shRNA (#1), and AAV-dsRed-pSico-*Cilk1* shRNA (Figure S2C), a synthetic double-stranded DNA fragment (Sigma-Aldrich) was inserted into the backbone plasmid pAAV2-dsRed-pSico-shRNA (a gift from Dr. Ronald S. Duman)[22] between the *Hpa*I/*Xho*I sites. For production of AAV-U6-GFP-scramble, AAV-U6-GFP-*Ift88* shRNA #1, and AAV-U6-GFP-*Ift88* shRNA #2 used to validate the *Ift88* shRNA sequences (Figures S5A and S5B), a synthetic double-stranded DNA fragment was inserted into the backbone plasmid pAAV2-U6-GFP (VPK-413, Cell Biolabs, San Diego, CA) between the *Bam*HI/*Eco*RI sites.

The inserted sequence (except the restriction enzyme recognition sequences) was scrambled sequence (5'-GCGCTTAGCTGTAG GATTCTTCAAGAGAGAATCCTACAGCTAAGCGCTTTTTT-3'), *Ift88* shRNA #1 (5'-GGCATTAGATACTTACAAATTCAAGAGATTTGTAA GTATCTAATGCCTTTTTT-3'), *Ift88* shRNA #2 (5'- GTATTTCCCTTCTAACATTTTCAAGAGAAATGTTAGAAGGGAAATACTTTTTT-3'), or *Cilk1* shRNA (5'-CACAACCACGTGGCGGTGTAATTCAAGAGATTACACCGCCACGTGGTTGTGTTTTTT-3'). The *Ift88* shRNA sequences were selected by referring to siDirect (http://sidirect2.rnai.jp). The *Cilk1* shRNA sequence is homologous to that previously

used in mice[37] with a 1-base difference. None of the shRNAs including the scrambled sequence caused any appreciable cytotoxicity or cell death when expressed in hypothalamic neurons (e.g., Figure S5D), suggesting that expression of the shRNAs did not cause saturation of the endogenous RNA interference pathway, which has been reported to induce neurotoxicity in the brain even with expression of a non-targeting (scramble) shRNA.[58]

To produce AAV-CMV-Flex-Flag-*Adcy3*^{M279I}, we designed the plasmid, pAAV2-CMV-Flex-Flag-*Adcy3*^{M279I} by referring to a previous study,[34] and then synthesized (Vector Builder, Yokohama, Japan).

The generated pAAV2 vectors were then used for the production and purification of the AAVs according to our methods,[56,59] and their final titrations were 8.8 × 10^{11} GC/ml (AAV2/1-Ef1α-DIO-palGFP), 3.3 × 10^{12} GC/ml (AAV2/1-dsRed-pSico-scramble), 2.4 × 10^{12} GC/ml (AAV2/1-dsRed-pSico-*Ift88* shRNA #1), 1.3 × 10^{12} GC/ml (AAV2/1-U6-GFP-scramble), 1.1 × 10^{12} GC/ml (AAV2/1-U6-GFP-*Ift88* shRNA #1), 1.1 × 10^{12} GC/ml (AAV2/1-U6-GFP-*Ift88* shRNA #2), 4.3 × 10^{14} GC/ml (AAV2/1-dsRed-pSico-*Cilk1* shRNA), and 4.3 × 10^{12} GC/ml (AAV2/1-CMV-Flex-Flag-*Adcy3*^{M279I}).

The AAV-dsRed-pSico-shRNA vectors, which ubiquitously label infected cells with DsRed, also express EGFP, but halt shRNA expression in Cre-negative cells. In Cre-positive cells, they do not express EGFP, but do express shRNA under the U6 promotor, thereby reporting Cre expression and permitting shRNA expression exclusively in Cre-expressing cells (Figures S2C and S2D).

Stereotaxic injection into the brain

Rats were anesthetized with a combination anesthetic (0.15 mg/kg medetomidine hydrochloride, 2.0 mg/kg midazolam, 2.5 mg/kg butorphanol tartrate; s.c.) following brief gas anesthesia with 3% isoflurane and were positioned in a stereotaxic apparatus so that the incisor bar level was adjusted until the lambda and bregma levels were equal. A glass micropipette (tip inner diameter: 15–30 μm) filled with a solution containing AAV was perpendicularly inserted into the DMH (coordinates: 3.0–3.1 mm caudal to bregma, 0.5 mm lateral to the midline, 8.1–8.3 mm ventral to the brain surface) or the PVH (1.7–1.8 mm caudal to bregma, 0.5 mm lateral to the midline, 7.5 mm ventral to the brain surface). For AAV injection into the brain of 3–4-week-old *Mc4r*-Cre rats (Figures S2D and S2E), the coordinates used were DMH: 2.4 mm caudal to bregma, 0.5 mm lateral to the midline, and 7.5 mm ventral to the brain surface; and PVH: 1.4–1.5 mm caudal to bregma, 0.5 mm lateral to the midline, and 7.4 mm ventral to the brain surface. The solution (100 nl/site) was pressure-ejected by using a Picospritzer III (Parker, Hollis, NH). All AAV injections were made bilaterally. For retrograde neural tracing, a solution of Alexa Fluor (Alexa) 594-conjugated CTb (1 mg/ml, 100 nl/site; C34777, Thermo Fisher Scientific) was pressure-injected into the rMR (2.7–3.0 mm posterior to the interaural line, on the midline, 9.5 mm ventral to the brain surface) of 9–11-week-old rats. The micropipette remained for 5 min after injection before it was withdrawn. After the injection, all incisions were sutured and disinfected with iodine, and ampicillin sodium (0.2 ml, 125 mg/ml) and atipamezole hydrochloride (250 μg/kg) solutions were injected into femoral muscles. The rats were housed at least 7 days under regular health check until subsequent procedure or experiments. None of the rats exhibited any signs of pain or discomfort during the surgical procedures or postoperative recovery. For anterograde and retrograde tracing, rats were injected with AAV-EF1α-DIO-palGFP or CTb, respectively, and then survived for 2 weeks until subsequent immunohistochemical procedure described below.

Development of anti-MC4R antibodies

Anti-MC4R antibodies were developed by K.N. in the Department of Morphological Brain Science, Graduate School of Medicine, Kyoto University in 2004. Peptides of N-terminal (N34 peptide: YTSLHLWNRSSHGLHGNASESLGKGHSDGGCYEQ) and C-terminal (C19 peptide: KEIICFYPLGGICELPGRY) parts of the rat MC4R protein were synthesized (Sigma-Aldrich) and 2 mg of each peptide was conjugated with 2 mg of maleimide-activated bovine serum albumin (Pierce, Rockford, IL) through the cysteine residues. The conjugated peptide solutions were emulsified with the same volume of Freund's complete adjuvant (Difco, Detroit, MI) and then were intracutaneously injected in equal amounts into two male and one female guinea pigs for the N34 peptide and two males and two females for the C19 peptide under anesthesia. One month later, the animals were immunized again with the same conjugated peptides in Freund's incomplete adjuvant. The sera were collected 10–14 days after the second immunization, and a crude γ-globulin fraction was obtained by ammonium sulfate fractionation. This fraction was subjected to affinity chromatography on a SulfoLink Coupling Resin (Pierce) conjugated with the respective peptide (2 mg peptide per ml resin). The polyclonal antibodies were eluted from the column with 0.1 M glycine–HCl (pH 2.5), and the eluate was neutralized with 1.0 M potassium phosphate buffer (pH 8.6). The anti-MC4R antibodies against the N-terminus and C-terminus used in the present study were obtained from female and male guinea pigs, respectively. The N- and C-terminal antigenic peptide sequences have 94% and 84% homology to the mouse sequences, respectively.

DNA transfection into cultured cells and MC4R immunocytochemistry

The coding sequence of rat *Mc4r* cDNA was amplified by PCR from rat brain cDNA and cloned into pcDNA3 (Invitrogen) between the *Bam*HI/*Xho*I sites. pcDNA3-MC4R or pcDNA3 (mock transfection) was transfected into HEK293T cells with a Lipofectamine 2000 transfection reagent (Thermo Fisher Scientific). After 48 h, the cells seeded on cover glasses were fixed with 4% formaldehyde in 0.1 M phosphate buffer (pH 7.4). After a rinse with phosphate-buffered saline (PBS), the cells were incubated overnight with one of the anti-MC4R guinea pig antibodies against the N-terminus and C-terminus (2 μg/ml) in an antibody incubation buffer containing 0.3% Triton X-100.[60] After a rinse, the cells were further incubated with Alexa488-conjugated goat antibody to guinea pig IgG (5 μg/ml; A11073, Thermo Fisher Scientific) for 1 h. The stained cells on cover glasses were thoroughly washed and mounted onto glass slides for fluorescence microscopy. For antigen absorption, the anti-MC4R antibodies (2 μg/ml) were premixed with the respective antigenic peptide (0.8 μg/ml).

Immunohistochemistry

Immunohistochemical procedures followed our previous studies.[21,60] Animals under anesthesia with the combination anesthetic were transcardially perfused with saline and then with 4% formaldehyde in 0.1 M phosphate buffer (pH 7.4). The brains were removed, postfixed in the fixative at 4°C for 2 h, and transferred into a 30% sucrose solution longer than overnight for cryoprotection. The tissues were cut into 30-μm-thick frontal sections on a freezing microtome and were subjected to immunohistochemical analyses. For immunostaining for VGLUT3, the fixative used for perfusion and postfixation was 2% formaldehyde in 0.1 M phosphate buffer (pH 7.4). For immunostaining for TRH, rats were perfused with 3% formaldehyde and 1% acrolein in 0.1 M phosphate buffer (pH 7.4), and the brains were postfixed in the same fixative without acrolein.

For immunoperoxidase staining for MC4R, brain sections were incubated overnight with guinea pig polyclonal antibodies against the N- or C-terminus of rat MC4R (2 μg/ml) and then for 1 h with biotinylated donkey antibody to guinea pig IgG (10 μg/ml; 706-065-148, Jackson ImmunoResearch, West Grove, PA). The sections were further incubated for 1 h with avidin-biotinylated peroxidase complex (ABC, 1:50; PK-6100, Vector Laboratories, Burlingame, CA). Bound peroxidase was visualized by incubating the sections in a Ni-DAB solution containing 0.02% 3,3′-diaminobenzidine tetrahydrochloride (DAB; Merck), 0.0002% hydrogen peroxide, and 0.5% ammonium nickel sulfate hexahydrate in 50 mM Tris-HCl (pH 7.6) to develop MC4R immunoreactivity as a blue-black reaction product of Ni-DAB. The sections were mounted on amino silane-coated glass slides and coverslipped. The sections were observed under a bright-field microscope. The anti-MC4R antibody to the N-terminus was used in the following MC4R immunostaining due to its better staining performance.

For double immunoperoxidase staining for palGFP and VGLUT3 for anterograde tracing, brain sections from the *Mc4r*-Cre rats that received an injection of AAV-EF1α-DIO-palGFP into the DMH were incubated overnight with anti-VGLUT3 guinea pig antibody (0.5 μg/ml)[53] and then for 1 h with biotinylated donkey antibody to guinea pig IgG (10 μg/ml). The sections were further incubated for 1 h with ABC (1:50). Bound peroxidase was visualized by incubating the sections with the Ni-DAB solution to develop VGLUT3 immunoreactivity as a blue-black reaction product. The bound peroxidase and unreacted avidin and biotin in the sections were blocked with 3% hydrogen peroxide and an avidin-biotin blocking kit (SP-2001, Vector Laboratories), respectively. The sections were further incubated overnight with anti-GFP mouse antibody (1 μg/ml; A11120, Thermo Fisher Scientific). After the sections were incubated with biotinylated donkey antibody to mouse IgG (10 μg/ml; AP192B, Merck) and then with ABC, the bound peroxidase was visualized by incubating the sections with 0.02% DAB and 0.001% hydrogen peroxide in 50 mM Tris-HCl (pH 7.6). In this manner, GFP immunoreactivity was developed as a brown reaction product of DAB. The sections were mounted on amino silane-coated glass slides and coverslipped.

For immunofluorescence staining for MC4R in combination with retrograde tracing, brain sections from the rats that were injected with Alexa594-conjugated CTb into the rMR were incubated overnight with anti-MC4R guinea pig antibody (2 μg/ml). After a rinse, the sections were incubated for 1 h with Alexa488-conjugated goat antibody to guinea pig IgG (5 μg/ml). CTb-labeled cells were identified by the fluorescence of Alexa594 combined with CTb.

For immunofluorescence staining for MC4R in sections with fluorescence labeling of neurons with DsRed, EGFP and/or palGFP, the sections were incubated overnight with anti-MC4R guinea pig antibody (2 μg/ml). After a rinse, the sections were incubated for 1 h with Alexa647-conjugated (A21450, Thermo Fisher Scientific) or Alexa594-conjugated (A11076, Thermo Fisher Scientific) goat antibody to guinea pig IgG (5 μg/ml).

For double immunofluorescence staining for MC4R and AC3, OXT or AVP, sections were incubated overnight with a combination of anti-MC4R guinea pig antibody (2 μg/ml) and anti-AC3 rabbit antibody (0.4 μg/ml; sc-588, Santa Cruz Biotechnology), anti-OXT rabbit serum (1:5000; 20068, Immunostar, Hudson, WI) or anti-AVP rabbit serum (1:5000; PC234L, Merck). After a rinse, the sections were incubated for 1 h with a combination of Alexa488-conjugated goat antibody to guinea pig IgG (5 μg/ml) and Alexa594-conjugated goat antibody to rabbit IgG (5 μg/ml; A11037, Thermo Fisher Scientific) or with a combination of Alexa488-conjugated goat antibody to rabbit IgG (5 μg/ml; A11034, Thermo Fisher Scientific) and Alexa594-conjugated goat antibody to guinea pig IgG (5 μg/ml).

For double immunofluorescence staining for MC4R and α-MSH, sections were incubated overnight with anti-MC4R guinea pig antibody (2 μg/ml) and anti-α-MSH sheep serum (1:10,000, AB5087, Merck). After a rinse, the sections were incubated for 1 h with Alexa488-conjugated donkey antibody to goat IgG (5 μg/ml; A11055, Thermo Fisher Scientific). The sections were blocked with 10% normal goat serum for 1 h and then incubated with Alexa594-conjugated goat antibody to guinea pig IgG (5 μg/ml).

For double immunofluorescence staining for MC4R and CRH, sections were incubated with anti-MC4R guinea pig antibody (2 μg/ml) and anti-CRH rabbit serum (1:10,000; T-4037, Peninsula Laboratories, San Carlos, CA) at 4°C for 2 days. After a rinse, the sections were incubated with biotinylated donkey antibody to rabbit IgG (10 μg/ml; AP182B, Merck) and Alexa594-conjugated goat antibody to guinea pig IgG (5 μg/ml) for 1 h. The sections were further incubated with ABC (1:50) for 1 h and then, CRH immunoreactivity was visualized by reaction with FITC-conjugated tyramide (1:50; SAT701001KT; Tyramide Signal Amplification FITC Systems, ParkinElmer) for 1 min.

For double immunofluorescence staining for MC4R and TRH, sections of rat brains perfused with the fixative containing formaldehyde and acrolein described above were treated with 1% sodium borohydride in distilled water for 30 min, and then with 0.5% H_2O_2 and 0.5% Triton X-100 in PBS for 15 min. After a rinse, the sections were incubated with anti-MC4R guinea pig antibody (2 μg/ml) and anti-TRH sheep serum (1:10,000; a gift from Dr. Csaba Fekete)[54] at 4°C for 2 days. After a rinse, the sections were incubated for 1 h with biotinylated donkey antibody to goat IgG (10 μg/ml; AP180B, Merck). After blocking with 10% normal goat serum

for 1 h, the sections were incubated with Alexa594-conjugated goat antibody to guinea pig IgG (5 μg/ml). The sections were further incubated with Alexa488-conjugated streptavidin (5 μg/ml; S11223, Thermo Fisher Scientific) for 1 h.

For immunofluorescence staining for IFT88, sections were incubated with anti-IFT88 rabbit antibody (0.8 μg/ml; 13967-1-AP, Proteintech, Rosemont, IL) overnight and then with biotinylated donkey antibody to rabbit IgG (10 μg/ml). The sections were further incubated with Alexa594-conjugated streptavidin (5 μg/ml; S11227, Thermo Fisher Scientific) for 1 h.

After fluorescence staining, sections were thoroughly washed and mounted onto glass slides. Following coverslipped with 50% glycerol/50% PBS containing 2.5% triethylenediamine, they were observed under an epifluorescence microscope (Eclipse 80i, Nikon) or a confocal laser-scanning microscope (TCS SP8, Leica).

In situ hybridization combined with immunohistochemistry

For histochemical measurement of intracellular *Cilk1* mRNA (Figure S7C), we performed fluorescence *in situ* hybridization for *Cilk1* mRNA using RNAscope Multiplex Fluorescent Reagent Kit v2 (323100, Advanced Cell Diagnostics, Newark, CA) combined with immunohistochemistry to detect EGFP and DsRed. Two weeks after injections of AAV-dsRed-pSico-*Cilk1* shRNA into the DMH and PVH, *Mc4r*-Cre rats were transcardially perfused with 4% formaldehyde as above. The brains were postfixed in the fixative at 4°C for 2 days, cryoprotected in a 30% sucrose solution longer than overnight, and sliced into 25-μm-thick frontal sections. The sections mounted on glass slides were dried at 60°C for 30 min and treated with hydrogen peroxide according to the manufacturer's (RNAscope) instructions. The slides were placed in 99.5% ethanol for 3 min and dried at room temperature for 5 min and then at 60°C for 30 min. The sections were treated with RNAscope Protease Plus at 40°C for 10 min and washed in distilled water 3 times. The sections were then treated with 0.1% Tween 20 in PBS at room temperature for 15 min and incubated with anti-GFP mouse antibody (1 μg/ml) and anti-monomeric red fluorescent protein (mRFP) rabbit antibody (1 μg/ml)[55] in 5× SSC at 4°C for > 17 h. The anti-mRFP antibody cross-reacted with dsRed. After a wash in PBS containing 0.1% Tween 20, the sections were incubated with Alexa488-conjugated goat antibody to mouse IgG (10 μg/ml; A11029, Thermo Fisher Scientific) and Alexa647-conjugated goat antibody to rabbit IgG (10 μg/ml; A21245, Thermo Fisher Scientific) in 5× SSC at room temperature for 2 h. After a wash in PBS containing 0.1% Tween 20, the sections were incubated with 4% formaldehyde at room temperature for 30 min to covalently conjugate the antibodies to the tissue. The sections were washed in PBS containing 0.1% Tween 20, rinsed in distilled water, and treated with RNAscope 1× Target Retrieval Reagent for 5 min according to the manufacturer's instructions. This treatment involved heating the sections to a boiling temperature, which completely eliminated autofluorescence of EGFP and DsRed in the tissue. The sections were then processed for hybridization and amplification using RNAscope probes according to the manufacturer's instructions using a negative control probe (310043, Advanced Cell Diagnostics) or a probe for mouse *Cilk1* mRNA (1177181-C1, Advanced Cell Diagnostics), which had a 19-bp hybridization sequence targeting a mouse sequence (996 bp) with 91% homology to rat *Cilk1* mRNA. After the step of incubation with RNAscope Multiplex FL v2 HRP-C1, the sections were incubated with Cy3-conjugated tyramide (1:200; NEL744001KT; TSA Plus Cyanine 3, Akoya Biosciences, Marlborough, MA) at 40°C for 30 min to develop mRNA hybridization signals. After washing with RNAscope Wash Buffer, the sections were treated with RNAscope HRP blocker at 40°C for 15 min to stop the reaction. After washing with RNAscope Wash Buffer and with PBS, the sections were dried in the dark at 4°C overnight and coverslipped as described above.

Hybridization with the negative control probe resulted in very low background signals, confirming the specificity of the remarkable dot signals with the probe for *Cilk1* mRNA (Figure S7C). RNAscope has single-molecule resolution, one dot of hybridization signal represents one transcript, and therefore the number of dots is considered proportional to the number of transcripts expressed.[61] We counted the number of dots within each cell body in the DMH and PVH in the sections and compared between the neuronal groups expressing both EGFP (Alexa488) and DsRed (Alexa647) (*i.e.*, *Mc4r*-Cre-negative cells that did not express *Cilk1* shRNA) and those expressing only DsRed (*i.e.*, *Mc4r*-Cre-positive cells that expressed *Cilk1* shRNA) (Figure S7C).

Measurement of ciliary length

For imaging analyses of primary cilia, z-series stacks of 291-μm-square and 25-μm-thick images were taken with a 40 × 1.3 NA oil objective using a z-resolution of 1 μm by a confocal laser-scanning microscope (TCS SP8, Leica). This confocal imaging was performed at defined locations (3 locations in the PVH and 1 location in the DMH; see Figure S3). To measure the length of primary cilia in the acquired images, we analyzed the confocal z-series stacks in an Imaris software (version 9.6.0, Oxford Instruments, Abingdon, UK) by tracing each fluorescence-labeled primary cilium either manually with the Filament tool or, when analyzing straight cilia, through semi-automated detection in Imaris, which created an artificial object encasing a cilium with the Surfaces function and then exported the length of the longest dimension of the object. We always visually verified that the semi-automated tracing was performed properly. We obtained the total length of all MC4R-immunoreactive primary cilia or all AC3-immunoreactive, MC4R-immunonegative primary cilia within a confocal z-series stack (*i.e.*, 291 × 291 × 25 μm imaged space). To obtain the total ciliary length in the PVH, we further summed the total lengths from the three imaged spaces in the PVH, except for Figure S5B, which shows the total length in one imaged space of the PVH.

To avoid undercounting $MC4R^+$ cilia lost due to aging or *Ift88* KD, and to avoid underestimating the length of cilia cut by tissue sectioning, we calculated the total ciliary length (as opposed to the average ciliary length per cell) when evaluating "remaining" $MC4R^+$ cilia within each hypothalamic region and compared it among groups of animals of different ages or treatments (e.g., Figure 3A), because the total length of remaining $MC4R^+$ cilia should represent the total melanocortin sensitivity of neurons within the tissue area. However, when comparing ciliary length between cell groups (e.g., MC4R-positive cilia *vs* MC4R-negative cilia in Figure 1C), we calculated the average length per cilium.

Measurements of body fat percentage, metabolism, and body surface area

Whole-body composition analysis to obtain body fat percentage was conducted using a quantitative magnetic resonance method without anesthesia (EchoMRI-900, Hitachi, Tokyo, Japan). To obtain whole-body metabolic rate, oxygen consumption rate, VO_2 (ml/min) was monitored for 48 h (over 3 days) using a metabolism-measuring system for small animals (MK-5000RQ; Muromachi Kikai, Tokyo, Japan). We analyzed average readings of VO_2 for a 24-h period (from 7:00 a.m. to 7:00 a.m.) on the second and third days, by which time the animals had adapted to the environment. In Figures 4B and 4F, VO_2 data during the light (7:00 a.m. to 7:00 p.m.) and dark (7:00 p.m. to 7:00 a.m.) periods were separately analyzed. Body surface area was calculated by Meeh's formula, $S = kW^{2/3}$ (S, body surface area; k, constant; W, weight) as previously reported.[62] To obtain the k value for the rat strain used in the present study, we first measured the body surface area of male Wistar/ST rats by a 3D scanner (Einscan SP, Japan 3D printer, Tokyo, Japan) under anesthesia with the combination anesthetic and then, calculated k values from the measured surface area and body weight as shown in Figure S4F. By using the obtained k values and Meeh's formula, we calculated the body surface area-to-mass (weight) ratios of the NC-fed rats for Figure 3D based on their body weight.

Measurement of food intake and dietary restriction

The amount (weight) of food intake was measured by placing rats individually in a cage installed with an automated feeding behavior measurement apparatus (Feedam, Melquest, Toyama, Japan). The cage had a water bottle and a food box containing NC (D12450H, Research Diets, New Brunswick, NJ) or HFD (D12451), and the access to the food box was time-controlled by a shutter. For *ad libitum* feeding, the shutter was opened all the time. For dietary restriction (DR), the shutter was opened at 5:00 p.m. every day and was closed when the food (NC) consumption reached 60% of the amount consumed by age-matched rats with *ad libitum* NC feeding.

Leptin resistance test

Male *Mc4r*-Cre rats aged 7 weeks were anesthetized with the combination anesthetic, and we drilled a small hole in the skull to access the lateral ventricle (0.8 mm caudal to bregma, 1.8 mm right to the midline and 3.8 mm ventral to the brain surface) and also injected AAV-dsRed-pSico-scramble or AAV-dsRed-pSico-*Ift88* shRNA bilaterally into both DMH and PVH or into PVH only. After the surgery, the incisions were sutured and disinfected with iodine, and ampicillin sodium (0.2 ml, 125 mg/ml) and atipamezole hydrochloride (250 μg/kg) solutions were injected into femoral muscles. The rats were individually caged under regular health check and their 24-h food intake (from 5:00 p.m. to 5:00 p.m.) was measured using Feedam with NC as described above. Two weeks after the AAV injections, 5 μl pyrogen-free 0.9% saline (Otsuka, Tokyo, Japan) was injected into the lateral ventricle with a microsyringe (Hamilton) at a rate of 5 μl/min under gas anesthesia with 3% isoflurane. One week later, another injection was made with 5 μl recombinant rat leptin (1 mg/ml; 598-LP, R&D Systems, Minneapolis, MN), which was dissolved in pyrogen-free 0.9% saline, into the lateral ventricle in the same manner. This dose of leptin has been shown to reduce food intake for 2 days in rats.[63] To exclude the effect of postanesthetic hypophagia, we waited at least 24 h after intracerebroventricular injection before initiating the measurement of 24-h food intake. The 24-h food intake after saline or leptin injection is expressed as a percentage of the average 24-h food intake during the 72-h period prior to each injection (Figure 6A).

Chronic leptin injection

Injection into the lateral ventricle through a pre-implanted cannula in free-moving rats was performed according to our previous procedure.[19] Recombinant rat leptin (5 μg in 5 μl) or saline was injected into the lateral ventricle of male Wistar/ST rats under the DR condition described above. The injection was performed at 01:00 p.m. every other day for 5 weeks starting at 12 weeks of age. At the end of the injection period, the rats were transcardially perfused with 4% formaldehyde as above, and the brains were processed for immunohistochemical analysis of the length of $MC4R^+$ cilia.

Measurement of serum leptin

Male Wistar/ST rats were raised in the NC, HFD, or DR condition in Feedam from 3 to 24 weeks of age as described above. Blood samples were collected from the tail at 3, 9, 15, and 24 weeks of age, and the leptin concentrations in the sera were measured using a Mouse/Rat Leptin Quantikine ELISA Kit (MOB00B, R&D Systems) according to the manufacturer's instructions. The correlation between the obtained average leptin concentrations and the total $MC4R^+$ ciliary length in the DMH of the rats of the same age and dietary conditions (data from Figure 3A) was analyzed (Figure 6D).

Quantitative real-time PCR

Male Wistar/ST rats aged 3 and 24 weeks were anesthetized with the combination anesthetic and quickly perfused with PBS transcardially. The brains were sliced and the PVH and DMH were separately dissected and stored in RNAlater (Merck) at –80°C. Total RNA was isolated with an RNeasy Lipid Tissue Mini Kit (Qiagen), according to the manufacturer's protocol. Reverse transcription from total RNA (0.4 μg) and qPCR were performed using an iTaq Universal SYBR Green One-Step Kit (Bio-Rad) in a StepOnePlus real-time PCR system (Thermo Fisher Scientific). All procedures were performed according to the manufacturers' protocols. The amount of *Mc4r* mRNA was normalized to that of β-actin mRNA and the relative fold mRNA expression was calculated by the delta-delta Ct method. Based on the sequences of rat *Actb* (β-actin) mRNA (NM_031144) and rat *Mc4r* mRNA (NM_013099), we used the primers for SYBR-green qPCR: *Actb*: forward 5'-CCACACTTTCTACAATGAGC-3' and reverse 5'-ATACAGGGACAACACAGC-3'; *Mc4r*: forward 5'-GACGGAGGATGCTATGAG-3' and reverse 5'-AGGTTCTTGTTCTTGGCTAT-3'.

Telemetry

Simultaneous telemetric recordings of activity, T_{core}, and T_{BAT} in free-moving rats were performed according to our procedure.[20] Briefly, male *Mc4r*-Cre rats, 7 weeks old, were anesthetized with the combination anesthetic and injected bilaterally into the DMH and PVH with AAV-dsRed-pSico-scramble or AAV-dsRed-pSico-*Ift88* shRNA as described above. The rats were then implanted with a battery-operated telemetric transmitter that projected two cables of external thermistor probes (F40-TT, Data Science International, St Paul, MN), one placed in the abdominal cavity to monitor T_{core} and the other inserted into the interscapular BAT. After surgery, all incisions were sutured and disinfected with iodine, and ampicillin and atipamezole were injected as described above. The rats were individually housed for 2 weeks to recover from surgery under regular health check. None of the rats exhibited any signs of pain or discomfort during surgery or postoperative recovery. During the recovery period, the animals were acclimated to the experimental environment.

On the day before data collection, the individually caged animals were placed in a climate chamber air-conditioned at 25 ± 1°C, and telemetric recordings of activity, T_{core}, and T_{BAT} were started by using a telemetry system (PhysioTel and PONEMAH, Data Science International). Circadian changes in the physiological variables were monitored for 48 h starting at 07:00 a.m. (Figures S5F and S5G). The effects of 4°C and 15°C exposure on T_{core}, and T_{BAT} were examined on separate days by changing the air temperature in the chamber (Figure S5G).

In vivo physiological experiment

In vivo physiological experiments were conducted as previously described.[64,65] Male Wistar/ST rats aged 9–11 weeks and 6 months and male *Mc4r*-Cre rats 2–4 weeks after bilateral injections of AAV-dsRed-pSico-scramble or AAV-dsRed-pSico-*Ift88* shRNA into the DMH at 9 weeks old were used. Rats were anesthetized with urethane (0.8 g/kg) and α-chloralose (80 mg/kg) after cannulation of a femoral artery, a femoral vein, and the trachea under anesthesia with 2%–3% isoflurane in 100% O_2. HR was recorded from a pressure transducer attached to the arterial cannula. T_{core} was monitored with a copper-constantan thermocouple inserted into the rectum and maintained at 36.0–38.0°C by perfusing a plastic water jacket, which was wrapped around the shaved trunk, with warm or cold water. Skin temperature was monitored with a thermocouple taped onto the abdominal skin underneath the water jacket. The rats were placed in a stereotaxic apparatus with a spinal clamp, paralyzed with D-tubocurarine (0.6 mg i.v. initial dose, supplemented with 0.3 mg/h), and artificially ventilated with 100% O_2 (60 cycles/min, tidal volume: 3.5 ml) to stabilize BAT nerve recording by preventing respiration-related movements. Mixed expired CO_2 (Exp. CO_2) was monitored through the tracheal cannula using a capnometer to provide an index of changes in whole-body metabolism. T_{BAT} was monitored with a needle-type thermocouple (0.33 mm diameter; Physitemp, Clifton, NJ) inserted into the left interscapular BAT pad, and postganglionic BAT SNA was recorded from the central cut end of a nerve bundle isolated from the ventral surface of the right interscapular BAT pad after dividing it along the midline and reflecting it laterally. The nerve bundle was placed on bipolar hook electrodes and soaked in mineral oil. Nerve activity was amplified (× 5,000–50,000) and filtered (1–300 Hz) by a CyberAmp 380 amplifier (Molecular Devices). All the physiological variables were digitized and recorded to a personal computer using a Spike2 software (version 7.10, CED, Cambridge, UK).

For nanoinjection into the brain, a sharp glass micropipette (tip inner diameter: 15–30 μm) filled with MTII (0.5 mM; M8693, Merck) dissolved in pyrogen-free 0.9% saline, was perpendicularly inserted and unilaterally injected into the DMH (100 nl). In experiments to examine the effect of neuronal inhibition in the rMR or periaqueductal gray/dorsal raphe nucleus on MTII-evoked physiological responses (Figures 2C–2E, and S2G–S2I), saline or muscimol was nanoinjected into the rMR (100 nl, midline single injection) or periaqueductal gray/dorsal raphe nucleus prior to MTII injection into the DMH. Periaqueductal gray/dorsal raphe nucleus injections were bilateral and at 4 sites at once (60 nl/site; coordinates: ventrolateral periaqueductal gray, 8.4–8.6 mm caudal to bregma, 0.8 mm left and right to the midline, 5.4 mm ventral to the brain surface; dorsal raphe nucleus, 7.5 mm caudal to bregma, 0.3 mm left and right to the midline, 5.5 mm ventral to the brain surface; corresponding to previous rat[24] and mouse[25] studies). Because two unilateral MTII injections into the left and right DMH elicited consistent physiological responses, the effects of saline and muscimol were tested sequentially in the same rats by injecting into the same sites > 1 h apart. To identify the injection sites, a small amount (~ 5 nl) of fluorescent microbeads (0.1 μm diameter, 0.2% solids in saline; F8801 or F8803, Thermo Fisher Scientific) was injected at the same site with the same pipette at the end of recordings. In experiments involving skin cooling-evoked BAT thermogenesis (Figures 5E and 5F), the trunk skin was cooled by perfusing the water jacket with ice-cold water for 1 min, which reduced the skin temperature by approximately 4°C from thermal conditions under which BAT SNA was very low (initial skin temperature, 37–39°C). After recordings, the animals were transcardially perfused with 4% formaldehyde and the brain tissues were processed for MC4R immunohistochemistry as described above.

For data analyses, BAT SNA amplitudes were quantified using Spike2 in sequential 4-s bins as the square root of the total power (root mean square) in the 0–20 Hz band of the autospectra of each 4-s segment of the BAT SNA traces. The "power/4 s" traces were used for quantification and statistical analyses of changes in BAT SNA. In experiments testing MTII-evoked physiological responses (Figures 2D, 2E, 5A–5D, S2H, and S2I), baseline values of BAT SNA, T_{BAT}, Exp. CO_2, and HR were the averages during the 30-s period immediately prior to MTII injection. MTII-induced changes in T_{BAT}, Exp. CO_2, and HR were calculated as changes from their baseline to peak values within 5 min after MTII injection. For MTII-induced changes in BAT SNA, the area under the curve (AUC) of the "power/4 s" trace above the baseline for 5 min after MTII injection was expressed as % of the area below the baseline for the 5-min period. In experiments involving skin cooling-evoked BAT thermogenesis (Figures 5E and 5F), baseline values of BAT SNA, T_{BAT}, Exp. CO_2, and HR were the averages during the 30-s period immediately prior to skin cooling. Skin cooling-evoked changes in T_{BAT}, Exp. CO_2, and HR were calculated as changes from their baseline to peak values within 100 s after the initiation of cooling. For skin cooling-evoked

changes in BAT SNA, the AUC of the "power/4 s" trace above the baseline for 100 s after the initiation of cooling was calculated as % of the area below the baseline for the 100-s period.

QUANTIFICATION AND STATICAL ANALYSIS

Anatomy and statistical analysis

We adopted the cytoarchitecture and nomenclature of most brain regions from Paxinos and Watson,[66] but those of subregions in the PVH followed a previous study.[67] The DMH consisted of the dorsomedial hypothalamic nucleus and dorsal hypothalamic area.[19,20] The raphe pallidus nucleus was nomenclaturally divided into the rostral (rRPa) and caudal parts at the rostral end of the inferior olivary complex.[21,68]

Data are shown as the means ± SEM. Statistic comparison analyses were performed using a paired or unpaired t test, simple linear regression, Pearson's correlation test, ordinary one-way ANOVA followed by Bonferroni's multiple comparisons test, and ordinary or repeated measures two-way ANOVA followed by Bonferroni's multiple comparisons test (Prism 7, GraphPad, La Jolla, CA), as indicated in the figure legends. All the statistic tests were two-sided. $p < 0.05$ was considered statistically significant. All results from ANOVA and t tests in main figures are shown in Table S1.